2D Hard Core Bosons Paradigm for Cuprates Superconductivity

Research Thesis

In Partial Fulfillment of the

Requirements for the

Degree of Master of Science in Physics

Shahaf.S Asban

*A*cknowledgments

I would like to thank Prof. Amit Keren for his guidance, support, patience and encouragement during my work in his group as well as teaching the essence of scientific work.

Special thanks to Gil Drachuk for helping me with my first steps in the research as well as endless, fruitful and inspiring conversations throughout the experience.

I also thank Meni Shay for his help with the measurement system and sample preparation, with high level of expertise, in a pleasant and patient way .

I thank Prof. Gad Koren, Tal Kirzhner and Montaser Naamneh for their guidance, help and usage in their laboratory facilities.

I thank the lab technicians, Dr. Leonid Iomin and Shmuel Hoida, for their help.

Thanks to all my friends in the research group of magnetism and low temperature for a time well spent.

Special thanks to my parents and family for endless support, moral and confidence

i

Contents

List of Figures

List of Figures

Abstract

The temperature dependence of the absolute resistivity of $YBa_2Cu_3O_{7-\delta}$, $La_{2-x}Sr_xCuO_4$, $Bi_2Sr_2Ca_{n-1}Cu_nO_{2n+4-x}$ and $(Ca_xLa_{1-x})(Ba_{1.75-x}La_{0.25+x})Cu_3O_y$ thin films is reported, with special attention to the resistivity slope near T_c and under T^*. The results are compared with the Lindner-Auerbach (LA) theoretical version of Homes's law $\frac{d\rho}{dT} = 77.378\frac{K_B}{n_q^2\hbar c^2}\lambda^2(0)$ where $\frac{d\rho}{dT}(T_c)$ is the slope of the resistivity at T_c, $\lambda(0)$ is the superconducting penetration depth at $T = 0$, and n_q is the carrier charge in units of e. Good agreement between theory and experiment on all materials is achieved for $n_q = 1.72\pm0.15$, which is very close to the expected $n_q = 2$ for Bosons. This finding indicates that the LA formula is self-consistent and supports the growing belief that cuprate superconductivity emerges from preformed cooper pairs.

1

HTS   High T_c Superconductor

GL   Ginsburg-Landau

HCB   Hard Core Bosons

BCS   Bardeen Cooper Schrieffer

SIS   Superconductor Insulator Superconductor (Junctions)

HP   Holstein Primakoff (Mapping)

RGP-FT   Relativistic Gross Pitaevskii Field Theory

BKT   Berezinskii Kosterlitz Thouless

μ**SR**   Muon Spin Resonance

NMR   Nuclear Magnetic Resonance

ESR   Electron Spin Resonance

R-T   Resistance Vs. Temperature

BEC   Bose-Einstein Condensation

Introduction

Two major discoveries were made at a very early stage in the study of cuprate super-conductivity. One is the Uemura relation for underdoped samples [26] : $T_c \propto \lambda^{-2}$ where T_c is the superconducting transition temperature and λ is the magnetic penetration depth. This relation was derived using the Muon spin rotation (μSR) technique. The second discovery was that for under and optimal doping, at temperatures T above T_c, the resistivity ρ obeys $\rho \propto T$. Later on Homes extended the Uemura relation and showed that a broader relation holds for both under and overdoped samples: $\rho_s(0) \propto \sigma(T_c)T_c$ where $\rho_s(0)$ is the superfluid density at zero temperature, and $\sigma(T_c) = 1/\rho(T_c)$ is the conductance at T_c [14]. This was achieved with optical conductivity. In many low doping models $\rho_s(0) \propto \lambda^{-2}(0)$ where $\lambda(0)$ is the penetration depth at zero temperature. For both Homes and Uemura laws to co-exist $\sigma(T_c)$ must be universal for all underdoped materials (at least from the optical viewpoint). Neither Uemura nor Homes predict the constant of proportionality in their laws. Then came Lindner and Auerbach (LA) and with the hard core boson (HCB) model managed to derive the relation $\rho(T) = 77.378 \left(\frac{\lambda(0)}{n_q} \right)^2 \frac{K_B T}{\hbar c^2}$ where the Boson charge $n_q = 2$, to four significant digits [19]. This LA derivation clearly generates the Homes law but is more general; it also captures the linear resistivity and provides the coefficient of proportionality. The HCB model is expected to be valid for temperature lower than $T*$ where pairs are suppose to start forming in the cuprates. Due to impurities, experimentally $\rho(T = 0) \neq 0$ in some cuprates. Therefore, it is more practical to write the LA law in a differential form $n_q^2 = 77.378 \frac{K_B}{\hbar c^2} \lambda^2(0)/\frac{d\rho}{dT}$. When comparing their model to Homes data, LA achieved an agreement on a logarithmic scale, which is not very accurate [19]. In this work we intend to check the LA law as accurately as possible. We use D.C. resistivity measurements versus T in films to determine $\frac{d\rho}{dT}$ in geometry and material independent form. We extract $\lambda(0)$ from the literature. Our strategy is to assume that the HCB have charge $n_q e$ (rather than $2e$) and use Eq. 96 in Ref. [19] to extract the experimental n_q.

Finding n_q similar to 2 would means that the HCB model is self-consistent, and a very good starting point for understanding the conductivity in the cuprates.

1 Theoretical Review

1.1 Homes's Law

Homes's law is an empirical relationship for high temperature superconductors between T_c, $\rho_s(0)$, and $\sigma_{D.C.}(Tc)$. The law was written by Homes as

$$\rho_s^\alpha(0) = 120\sigma_{D.C.}^\alpha(Tc)T_c \tag{1}$$

where α denotes the crystallographic direction in case of anisotropic superconductors [13][14]. Homes's law holds for copper-oxide HTS's regardless of doping level or dopants kind (electrons-holes) as presented in Fig. 1 [[13]].
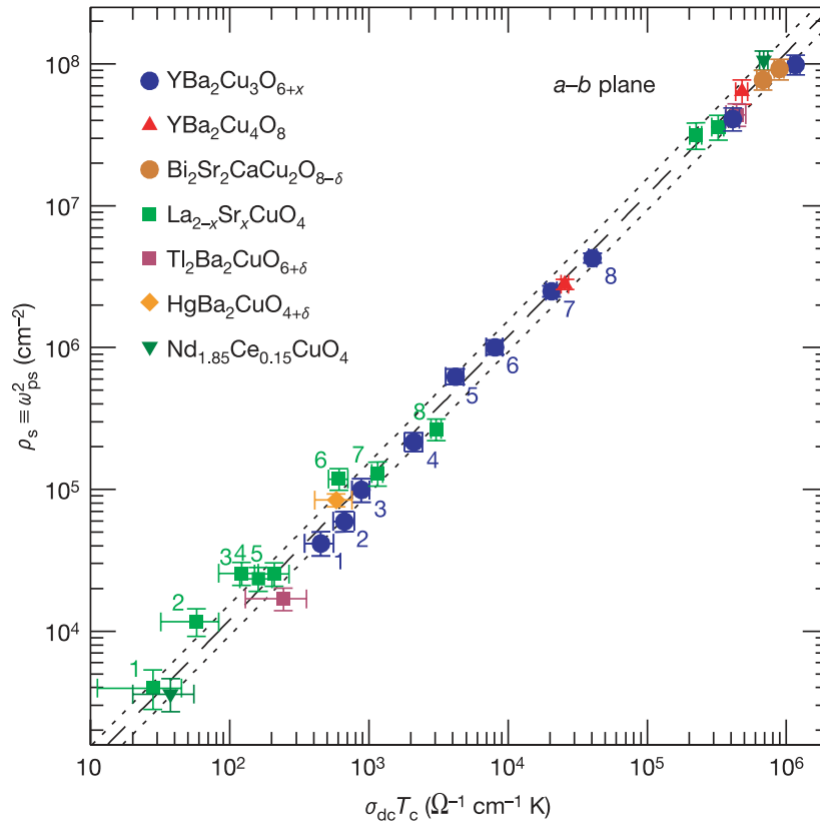

Figure 1: *shown Homes's law as presented in the famous publication of July 29th 2004 .[13]*

The uniqueness of this relationship originates from the fact that it connects physical quan-

tities of the condensate well below T_c and above, offering a notion of universal scaling law. Regarding the a-b plane conductivity, Homes assumes [14] that all of the spectral weight (the area obtained from the integral of the optical conductivity) of the free carriers in the normal state (n_n) collapses to the condensate below T_c $(n_n \equiv n_s)$ .Also, the low frequency conductivity close to T_c from above, may be described well by the Drude conductivity for metal $\sigma_1 (\omega) = \frac{\sigma_{D.C.}}{1+\omega^2 \tau^2}$ according to Homes which in this work approximates the spectral weight (area of the Lorenzian) to $\frac{\sigma_{D.C.}}{\tau}$. From Transport and reflectance measurements on copper-oxides Homes found the D.C conductivity by fitting to the Lorenzian. According to J.Orenstein [20] the scattering rate $1/\tau$ near the transition scales linearly with T_c, so the in-plane (a-b) conductance and the condensate strength scales to $\rho_s^\alpha(0) \propto \sigma_{D.C.}^\alpha(Tc)T_c$. In the c-axis, it is conceded that transport is incoherent and hopping governs the physics, this motivates the picture of a Josephson-coupling description for the inter layer conductivity. Homes in his work extracted the c-axis penetration depth by measurement of the critical current J_c and using the relations $\lambda^2 = \frac{\hbar c^2}{8\pi a_c e J_c}$ where a_c is the layer separation in the c-axis from which ρ_s is extracted. Using the relations $J_c = (\pi\Delta/2eR_n)\tanh(\Delta/2K_BT)$ where Δ is the superconducting energy gap, and $R_n = a_c/\sigma_{D.C.}$, he scaled the D.C. conductivity with the superfluid density and T_c in the c-axis as well.

1.2   The London Equation

Here we explain the concept of superfluid carrier density. One of the prominent features of the superconducting state is the absolute screening of a static magnetic field; the *Meisner effect*. The calculations done in the London framework provide a good approximation to the microscopic picture avoiding the details of the Ginsburg-Landau (GL) or the more basic BCS theory for the classic superconductors type I which reduces to the London theory once fixing ρ_s to a constant in real space (no fluctuations in charge density). The London theory takes the penetration depth $\lambda(T)$ and the critical field $H_c(T)$ as input parameters, hence provides only a phenomenological explanation for the *Meisner effect.*

6

The main assumption in this theory is that the classical vector potential $\vec{A}$ is proportional to the current density $\vec{J}$ [25] through a proportionality quantity ρ_s which is defined as the superfluid density

$$\vec{J} = \frac{\rho_s e^2}{mc} \vec{A} \tag{2}$$

hence,

$$\vec{\nabla} \times J = \frac{\rho_s e^2}{mc} \vec{B} \tag{3}$$

according to Maxwell's Eq.

$$\vec{\nabla} \times \vec{B} = \frac{4\pi}{c} \vec{J} \tag{4}$$

applying the curl on Maxwell's Eq.

$$\vec{\nabla} \times \vec{\nabla} \times \vec{B} = \nabla^2 \vec{B} - \underbrace{\nabla \left(\vec{\nabla} \cdot \vec{B} \right)}_{0} = \frac{4\pi e^2 \rho_s}{mc^2} \vec{B} \tag{5}$$

Thus,

$$\nabla^2 \vec{B} = \frac{4\pi e^2}{mc^2} \rho_s \vec{B} \tag{6}$$

For a sample on the ZoY plane with applied field on the z direction, a solution in the x direction would be

$$B_z (x) = B_0 e^{-x/\lambda} \tag{7}$$

when $\frac{1}{\lambda^2} = \frac{4\pi e^2 \rho_s}{mc^2}$, an exponential decay of the field inside the superconductor.

There are many ways to measure the penetration depth λ, including microwave reflection [8, 11], NMR [18] magnetic susceptibility measurement [10] and many more. The most

accurate is the Low Energy Muon Spin Resonance LE-μSR [17]. A low energy ray of muons at the required intensity is generated from two body pion decay. When high energy protons (over 500 MeV) collides the target nuclei of light element such as carbon or beryllium, it maximizes the production of π_+which life time is around $26 \times 10^{-6}[sec]$, followed by a decay to Muon and Muon neutrino as shown in Fig. 2.
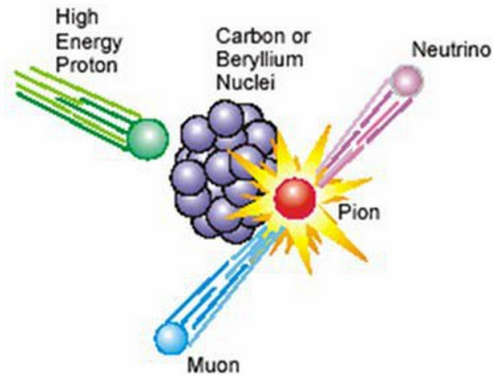
Figure 2: *Muon Ray Production process*

In this method, a ray of sufficiently slow muons is aimed towards the target material arriving nearly 100% spin polarized. When the Muon decays it emits a positron preferentially at the direction of its spin. From the anisotropy of the positron distribution, the spin polarization of the Muon ensemble's statistical average can be deduced, hence, the local field is estimated.

1.3 Hard Core Bosons, A model for cuprates superconductivity

Hard Core Bosons (HCB) model originates in recent studies that have shown very short coherence length ξ [15] for superconductors of the cuprate family (HTS's) in comparison to the unit cell size. The coherence length is usually deduced from the upper critical field H_{c2}.The coherence length is given by $H_{c2} = \frac{\phi_0}{2\pi\xi_0^2}$ where $\phi_0 = \frac{h}{2e}$ is defined as the flux quanta. In some cases, such as YBCO, $(H_{c2} > 100[T]$ @4.2$[K])$ as shown in [30][5], *Fig. 3* is extrapolated from the MF formula $\xi(T) = \frac{\xi(0)}{\left[1-\frac{T}{T_c}\right]^{1/2}}$. This gives a typical value of
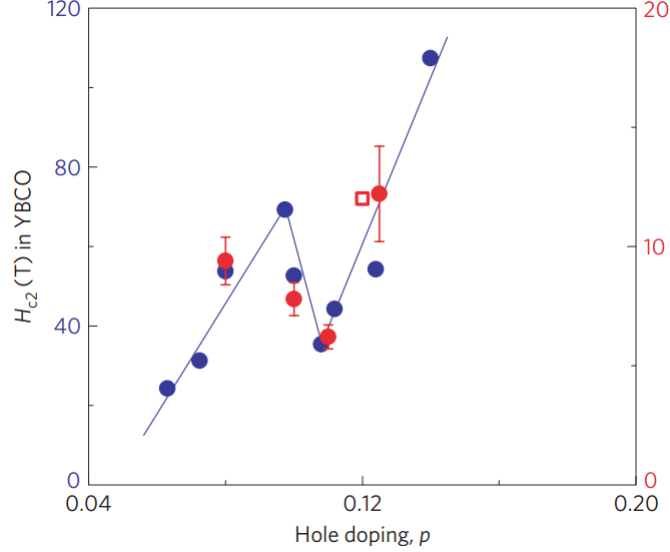
Figure 3: *Critical Field H_{C2} in YBCO as a function of doping [5]*

about $\tilde{\ }20[\overset{o}{A}]$ which is around 5 lattice sites (a = 3.82 Å, b = 3.89 Å, and c = 11.68 Å) at zero temperature.

Those observations imply, that the spatial separation of paired electrons in HTS's is within a few lattice-constant scale.

One way of understanding/achieving superconductivity effective model, is considering a strong attractive interaction between 2 charge carriers of the same kind. This attractive interaction must overcome the coulomb repulsion interaction, and could be mediated by lattice deformations (phonon) or spin fluctuations (magnons). Once the idea of a low energy bound state of 2 electrons is accepted, the Bose-Einstein statistics may be applied, and a condensate of such bound states would be a useful idea providing an intuitive explanation for superconductivity at high temperatures.

1.3.1 The Boson Hubbard Model

We now introduce the Boson Hubbard model; an effective model originated from the strong coupling regime of the fermionic Hubbard model presented in appendix A and B. The Boson Hubbard model is an approximated model that describes the dynamics of a

9

bosonic particles on a lattice in terms of annihilation and creation operators. The kinetic term is coupled with the letter J and describes the transfer of the bosons on a lattice between nearest neighbors annihilating the boson in site j and creating a boson in site i as shown in Eq. 8

$$\mathcal{H} = -2J\sum_{\langle i,j\rangle} \left(b_i^\dagger b_j + h.c. \right) - \mu\sum_i \hat{n}_i + \sum_{\langle i,j\rangle} J_{ij}^{int}\hat{n}_i\hat{n}_j \tag{8}$$

The second term coupled to the chemical potential and descries the energy of a site by adding/removing a particle summed all over the lattice, where $\hat{n} = b^\dagger b$ counts the number of particles at each site, in the HCB model $\hat{n}_i = \{0,1\}$ supporting exclusion. The last term introduces the *Ising anisotropy* coupling term and accounts for site-site interaction for anisotropic material. In some cases this model may be mapped into a model of spins on a lattice as elaborated below.

1.3.2 Holstein-Primakoff Mapping of the HCB model

The Holstein-Primakoff suggested the mapping from spin raising and lowering opera-tors, $\{S^+, S^-, S^z\}$ to creation annihilation operators $\{b^\dagger, b\}$. The transformation is pos-sible under the assumption of low temperatures, thus low probability for high excited states/occupancies to exist. It is done with respect to $1/s$ as a small parameter (even though in our case s=1/2, it is still relevant). According to Holstein-Primakoff we get

$$S_i^+ \to (2s)^{1/2}\left(1 - \frac{\hat{n}_i}{2s}\right)^{1/2} b_i \tag{9}$$

$$S_i^- \to (2s)^{1/2} b_i^\dagger \left(1 - \frac{\hat{n}_i}{2s}\right)^{1/2} \tag{10}$$

$$S_i^z \to s - \hat{n}_i \tag{11}$$

Given this transformation, the multiplication rule remains with similar structure, $\left[b_i, b_j^\dagger\right] = \delta_{ij} \rightsquigarrow \left[S_i^+, S_j^-\right] = 2\delta_{ij}S^z$, as claimed.

Now let us apply the HP transformation on a specific Hamiltonian which will serve the HCB model

$$\mathcal{H} = -\sum_{i \neq j} J_{ij} S_i^- S_j^+ \tag{12}$$

$$= -\sum_{i \neq j} J_{ij} \left[(2s)\, b_i^\dagger \left(1 - \frac{b_i^\dagger b_i}{2s}\right)^{1/2} \left(1 - \frac{b_j^\dagger b_j}{2s}\right)^{1/2} b_j \right] \tag{13}$$

Now perform approximation with respect to large S to first order in $1/s$

$$\mathcal{H} = E_0 - 2s \sum_{i \neq j} J_{ij} b_i^\dagger b_j + O\left(b^4\right) \tag{14}$$

when $E_0 = -s^2 \sum_{i \neq j} J_{ij}$ and b^4 correction are neglected. In this case the HCB is mapped into the spin Hamiltonian (20)

$$\mathcal{H} = -2J \sum_{\langle i,j \rangle} S_i^\perp \cdot S_j^\perp - \mu \sum_i S_i^z + \sum_{\langle i,j \rangle} J_{ij}^{int} S_i^z S_j^z \tag{15}$$

where $S^\perp = (s_x, s_y)$ and a quantum XY model is achieved.

1.3.3 Electromagnetic Coupling in the HCB

Discussing the paired fermions creating additive spin zero Bosons, the Zeeman term trivially vanishes and the coupling to the classical field is carried via the kinetic term alone. Consider the one particle Hamiltonian *schrödinger's* kinetic term in magnetic field

$$\mathcal{H} = \frac{\left(\vec{p} - q\vec{A}\right)^2}{2m} \tag{16}$$

under the transformation

$$\vec{p} - qA \to \vec{p}$$

$$|\psi'\rangle \to e^{-\frac{iq}{\hbar} \int \vec{A} \cdot d\vec{x}} |\psi_0\rangle$$

the eigen problem becomes

$$\mathcal{H}_k |\psi_0\rangle = \frac{\left(\vec{p} - q\vec{A}\right)^2}{2m} |\psi_0\rangle = E|\psi_0\rangle \to \mathcal{H}_k'|\psi'\rangle = \frac{\vec{p}^2}{2m}|\psi'\rangle = E|\psi'\rangle \tag{17}$$

instead of the minimal coupling, we let the wave function accumulate additive phase between spatially separated locations and gain the ability to use the same Hamiltonian as in the case of $\vec{A} = 0$.

Proof

$$\vec{p}\left(e^{-\frac{iq}{\hbar} \int \vec{A} \cdot d\vec{x}} \psi_0\right) = -i\hbar e^{-\frac{iq}{\hbar} \int \vec{A} \cdot d\vec{x}} \left(-\frac{iq}{\hbar} \vec{A}\psi_0 + \nabla\psi_0\right) \tag{18}$$

$$\vec{p}\left(e^{-\frac{iq}{\hbar} \int \vec{A} \cdot d\vec{x}} \psi_0\right) = e^{-\frac{iq}{\hbar} \int \vec{A} \cdot d\vec{x}} \left(\vec{p} - q\vec{A}\right) \psi_0 \tag{19}$$

Therefore,

$$\langle\psi'|\mathcal{H}_k^{A=0}|\psi'\rangle = \langle\psi_0|\mathcal{H}_k^{A\neq0}|\psi_0\rangle = E \tag{20}$$

up to a global phase the states are equivalent and the observables are identical. Translating this symmetry to the kinetic term of the Hubbard model we achieve

$$b_i^\dagger b_j \to e^{\frac{iq}{\hbar} A_{ij}} \tilde{b}_i^\dagger \tilde{b}_j$$

when,

$$A_{ij} = \int_{r_j}^{r_i} \vec{A \cdot} d\vec{r}$$

a particle is destroyed at r_j and created at r_i according to the creation/annihilation operators,while accumulating the phase dictated by the applied vector potential along that path.

Coupling the HCB model to electromagnetic field, the kinetic term acquire phase while propagating

$$\mathcal{H}_k^{HCB} = -2J\sum_{\langle i,j \rangle} e^{\frac{iq}{\hbar}A_{ij}} \tilde{b}_i^\dagger \tilde{b}_j + h.c. \underbrace{=}_{HPT} -2J\sum_{\langle i,j \rangle} e^{\frac{iq}{\hbar}A_{ij}} S_i^+ S_j^- + h.c. \tag{21}$$

hence, derivation for the kinetic term in the Hubbard model coupled to the vector potential. At this stage, we can verify the London hypothesis regarding Eq. 2. the quantum mechanical current density term in real space may be written in the presence of the vector field as

$$\vec{J} = \frac{q\hbar}{2mi}\left\{\psi^*\nabla\psi - \psi\nabla\psi^*\right\} - \frac{q^2}{m}A\psi^*\psi \tag{22}$$

Relying on the fact that there is no Zeeman term in our Hamiltonian we can also show that the variational derivative of the kinetic term with respect to the vector field leads to the same current density

$$E = \int \psi^* \frac{(\nabla - iqA)^2}{2m}\psi d^3x \tag{23}$$

$$\frac{\delta E}{\delta A} = -\frac{q\hbar}{2mi}\left\{\psi^*\nabla\psi - \psi\nabla\psi^*\right\} + \frac{q^2}{m}A\psi^*\psi = -\vec{J} \tag{24}$$

on the other hand

$$\frac{\delta E}{\delta A} = \rho_s \frac{q^2}{m^*}A \rightarrow \frac{\delta^2 E}{\delta A^2} = \rho_s \frac{q^2}{m^*} \tag{25}$$

13

According to Eq. 25, one may calculate the superfluid density which is also the condensate density $\psi^\dagger \psi = n_s$ in the framework of the HCB model by variation of the energy w.r. to the vector field.

1.3.4 The Current Density Operator in the HCB model

We now explain who conductivity is calculated in the HCB model. Our frame of work here describes strongly interacting electrons with the coupling constant U, perturbed with the kinetic term of energy t which allows the HCB to hop between any two adjacent lattice cells. First we will define the momentum span for the creation/annihilation operators

$$b_k = \frac{1}{\sqrt{N}}\sum_i b_i e^{ikr_i}$$

$$b_k^\dagger = \frac{1}{\sqrt{N}}\sum_i b_i^\dagger e^{-ikr_i}$$

and the reverse transformation

$$b_i = \frac{1}{\sqrt{N}}\sum_k b_k e^{-ikr_i}$$

$$b_i^\dagger = \frac{1}{\sqrt{N}}\sum_k b_k^\dagger e^{ikr_i}$$

By writing the kinetic term we get the dispersion

$$\mathcal{H}_k = \frac{-tJ}{N}\sum_{k,k',\langle i,j\rangle} e^{i(kr_i - k'r_j)} b_k^\dagger b_k + h.c. \tag{26}$$

in one dimension to get the current in the x coordinate for example we will get

$$\mathcal{H}_k = -2J\sum_k \cos(ka) b_k^\dagger b_k + h.c. \tag{27}$$

the phase velocity is the derivative w.r. to k

$$v_{phase}^x = \frac{1}{\hbar}\frac{\partial E_k}{\partial k} = \frac{-2J}{\hbar}\sum_k \underbrace{(-a\,sin\,(ka))}_{0} + cos\,(ka)\left[\frac{\partial b_k^\dagger}{\partial k}b_k + b_k^\dagger\frac{\partial b_k}{\partial k}\right] \qquad (28)$$

by plugging in the reverse transformation we get

$$v_{phase}^x = \frac{-i2tJa}{\hbar}\sum_{\langle i,j\rangle} b_i^\dagger b_j - b_j^\dagger b_i \qquad (29)$$

remembering the number operator this is the number of particals moving in the positive direction of the x coordinate subtracted the number of particals moving in the negative direction. Therefore the current density operator is given by

$$J^x = -2\frac{iJaq}{\hbar}\sum_{\langle i,j\rangle} b_i^\dagger b_j - b_j^\dagger b_i \qquad (30)$$

Applying again the the HP mapping we get the spin operator version of the Current Density

$$J^x = -2\frac{iJaq}{\hbar}\sum_{\langle i,j\rangle} b_i^\dagger b_j - b_j^\dagger b_i = -2\frac{iJaq}{\hbar}\sum_{\langle i,j\rangle} S_i^+ S_j^- - S_j^+ S_i^- = 4\frac{Jaq}{\hbar}\sum_{\langle i,j\rangle} S_i^x S_j^y - S_i^y S_j^x \quad (31)$$

Finally summing on spatial dimensions, the lattice constant a may be inserted into the summation index r

$$J^x = 4\frac{Jq}{\hbar}\sum_r S_r^x S_{r+x}^y - S_r^y S_{r+x}^x \qquad (32)$$

and the Current operator of the HCB is obtained.

15

1.3.5 Conductivity and Current Correlations

The linear response expression for current density is defined by the spatial/time convolution integral

$$\mathbf{J}\left(\mathbf{r},t\right) = \int_{-\infty}^{t} dt' \int d\mathbf{r}' \overline{\sigma}\left(\mathbf{r}-\mathbf{r}',t-t'\right)\mathbf{E}\left(\mathbf{r}',t'\right) \tag{33}$$

while the interaction that governs the dynamics is given by

$$\mathcal{V} = -\frac{1}{c}\int \mathbf{J}\cdot\mathbf{A}d\mathbf{r} \tag{34}$$

while

$$\mathbf{E} = -\frac{1}{c}\frac{\partial\mathbf{A}}{\partial t} \tag{35}$$

For a vector potential of the form

$$\mathbf{A}\left(\mathbf{r},t\right) = \mathbf{A}_0 e^{i(\mathbf{q}\mathbf{r}-\omega t)} \tag{36}$$

we get the relations

$$\mathbf{E} = \frac{i\omega}{c}\mathbf{A} \tag{37}$$

and we get

$$\mathbf{J}\left(\mathbf{r},t\right) = \frac{i\omega}{c}\int_{-\infty}^{t} dt' \int d\mathbf{r}' \overline{\sigma}\left(\mathbf{r}-\mathbf{r}',t-t'\right)\mathbf{A}\left(\mathbf{r}',t'\right) \tag{38}$$

Now let us see the dynamics for our vector potential

$$\mathcal{V} = -\frac{1}{c}\int \mathbf{A}\left(t\right)\mathbf{J}\left(r\right)e^{i\mathbf{q}\mathbf{r}}d\mathbf{r} = -\frac{V}{c}\mathbf{A}\left(t\right)\mathbf{J}\left(-q\right) \tag{39}$$

by the Fourier transformation defined as

$$\mathbf{J}\left(\mathbf{q}\right) = \frac{1}{V}\int\mathbf{J}\left(\mathbf{r}\right)e^{-i\mathbf{q}\mathbf{r}} \qquad (40)$$

Applying perturbation theory the evolution operator to first order

$$\mathbf{J}\left(\mathbf{q},t\right) = U^{\dagger}\left(t\right)\mathbf{J}\left(\mathbf{q}\right)U\left(t\right) \underset{2^{nd}order}{=} \mathbf{J}^{I}\left(\mathbf{q},t\right) + \frac{1}{i\hbar}\int_{-\infty}^{t}\left[\mathbf{J}^{I}\left(\mathbf{q},t\right),\mathcal{V}^{I}\left(t'\right)\right]dt' \qquad (41)$$

where

$$\mathbf{J}^{I}\left(\mathbf{q},t\right) = e^{\frac{i}{\hbar}\mathcal{H}_0 t}\mathbf{J}\left(\mathbf{q}\right)e^{-\frac{i}{\hbar}\mathcal{H}_0 t} \qquad (42)$$

and

$$\mathcal{V}^{I}\left(t\right) = -\frac{V}{c}\mathbf{A}\left(t\right)e^{\frac{i}{\hbar}\mathcal{H}_0 t}\mathbf{J}\left(-\mathbf{q}\right)e^{-\frac{i}{\hbar}\mathcal{H}_0 t} = -\frac{V}{c}\mathbf{A}\left(t\right)\mathbf{J}^{I}\left(-\mathbf{q},t\right) \qquad (43)$$

allowing only $\left[\mathbf{A}\left(\mathbf{t}\right),\mathcal{H}_0\right] = 0$, i.e., a classical field. Taking the thermal average on these quantities we achieve

$$\langle\mathbf{J}_{\alpha}\left(\mathbf{q},t\right)\rangle = \langle\mathbf{J}_{\alpha}^{I}\left(\mathbf{q},t\right)\rangle + \frac{V}{i\hbar c}\int_{-\infty}^{t}\langle\left[\mathbf{J}_{\alpha}^{I}\left(\mathbf{q},t\right),\mathbf{J}_{\beta}^{I}\left(-\mathbf{q},t'\right)\right]\rangle A_{\beta}\left(t'\right)dt' \qquad (44)$$

Since the first term exists for zero field, we deduce it represents persistent currents. we will continue further analysis considering the main interest, excitation of current with external field, $\langle\mathbf{J}_{\alpha}^{I}\left(\mathbf{q},t\right)\rangle = 0$. On the other hand, let us return to our initial definition of the current density using the chosen field A

$$\mathbf{J}\left(\mathbf{r},t\right) = \frac{i\omega}{c}\int_{-\infty}^{t}dt'\int d\mathbf{r}'\overline{\sigma}\left(\mathbf{r}-\mathbf{r}',t-t'\right)e^{-i\mathbf{q}(\mathbf{r}-\mathbf{r}')}\mathbf{A}\left(t'\right)e^{i\mathbf{q}\mathbf{r}} = \frac{i\omega V}{c}\int_{-\infty}^{t}dt'\overline{\sigma}\left(\mathbf{q},t-t'\right)\mathbf{A}\left(t'\right)e^{i\mathbf{q}\mathbf{r}}$$
$$(45)$$

from which we may extract $\mathbf{J}\left(\mathbf{q},t\right)$ as

$$\mathbf{J}\left(\mathbf{q},t\right)=\frac{i\omega V}{c}\int_{-\infty}^{t}dt'\overline{\sigma}\left(\mathbf{q},t-t'\right)\mathbf{A}\left(t'\right) \tag{46}$$

and by comparing to our thermally averaged formula we get

$$\sigma_{\alpha\beta}\left(\mathbf{q},t-t'\right)=\frac{1}{\hbar\omega}\langle\left[\mathbf{J}_{\alpha}^{I}\left(\mathbf{q},t\right),\mathbf{J}_{\beta}^{I}\left(-\mathbf{q},t'\right)\right]\rangle \tag{47}$$

defining the Time domain Fourier transform on positive times only assuming the perturbation begins at $t=0$ we get

$$\overline{\sigma}_{\alpha\beta}\left(\mathbf{q},\omega\right)=\frac{1}{\hbar\omega}\int_{0}^{\infty}\langle\left[\mathbf{J}_{\alpha}^{I}\left(\mathbf{q},t\right),\mathbf{J}_{\beta}^{I}\left(-\mathbf{q},0\right)\right]\rangle e^{i\omega t}dt \tag{48}$$

Finally using the results of appendix C we get the fluctuation-dissipation relations

$$\frac{2}{\hbar\omega}tanh\left(\frac{\beta\hbar\omega}{2}\right)\int_{-\infty}^{\infty}\langle\{\mathbf{J}_{\alpha}^{I}\left(\mathbf{q},t\right),\mathbf{J}_{\beta}^{I}\left(-\mathbf{q},0\right)\}\rangle e^{i\omega t}dt=\sigma_{\alpha\beta}\left(\mathbf{q},\omega\right)+\sigma_{\beta\alpha}^{\dagger}\left(\mathbf{q},\omega\right) \tag{49}$$

when $\{\cdot\}$stands for the anticommutator.

1.3.6 The Auerbach-Lindner HCB conductivity

Considering Eq. 32, 49, the conductivity may be calculated in the framework of the HCB model.

Using the Relativistic Gross-Pitaevskii Field Theory (RGP-FT) and Variational Harmonic Oscillator (VHO) up to 12^{th}moment [19], LA have shown that at high temperatures the two dimensional resistivity ρ^{2D} is approximated by

$$\rho^{2D}\left(T\right)=0.23R_{Q}\frac{T}{J}\left[1-2.9\left(\frac{J}{T}\right)^{2}+\mathcal{O}\left(\frac{J}{T}\right)^{4}\right] \tag{50}$$

$$R_{Q}=\frac{h}{(n_{q}e)^{2}} \tag{51}$$

18

where n_q is the Bosons charge. They also have shown that the two dimensional superfluid stiffness $\rho_s^{2D}(0) = 1.078J$. Alternatively, to first order in $1/T$, this can be written as

$$\frac{d\rho^{2D}}{dT} = 0.245 \frac{R_Q}{\rho_s^{2D}(0)}. \tag{52}$$

From this formula, and $\sigma^{2D} = 1/\rho^{2D}$, a natural HCB version of Homes's law

$$\rho_s^{2D}(0) = 0.245 \sigma^{2D}(T_c) T_c \tag{53}$$

arises, provided that $\rho^{2D}(0) = 0$. To relate the two dimensional quantities to the multi-layer 3D systems, we define the 2D critical conductance using the measured 3D resistivity by

$$\sigma^{2D} = \frac{a_c}{\rho} \tag{54}$$

where a_c is the inter plane distance.

Similarly the zero temperature 2D Boson superfluid stiffness is given by

$$\rho_s^{2D} = a_c \rho_s^{3D} = \frac{(\hbar c)^2}{16\pi e^2} \frac{a_c}{\lambda_{ab}^2} \tag{55}$$

where λ_{ab} is the London penetration depth when the applied field is perpendicular to the plane.

Eq. 52 leads to a relation between resistivity derivative, penetration depth, and the Bosons charge given by

$$\frac{d\rho}{dT} = 77.378 \frac{K_B}{n_q^2 \hbar c^2} \lambda^2(0) \tag{56}$$

Eq. 56 is the main equation which we use to analyze our data, where n_q^2 arose from the definition of quanta of resistance written in 51 .

1.4   Four Point Probe sheet resistivity Measurement Method

Resistivity measurement is the cardinal technique in this thesis. Due to that understanding, it was important for us to see first that we can measure absolute resistivity of thin films with small variation as possible due to different geometries, heights and even system of measurement. The main technique for that purpose is based on F.M. Smits's[22] article, Measurement of Sheet Resistivity with the Four-Point Probe. First, we will establish the underlying understanding of the method.

Imagine a current source (injector) in contact with 2d infinite conducting plane at a point set as the origin of a polar coordinate system. The current density at a distance r from the source is given by $j = \frac{I}{2\pi r}$. The electric field on the conducting surface is set by $\vec{j} = \sigma \vec{E}$. This necessitates a logarithmic potential

$$\varphi - \varphi_0 = -\frac{I\rho}{2\pi} ln\left(r\right) \tag{57}$$

where $\rho = 1/\sigma$ is the 2d sheet resistivity and φ is the electric potential. In a dipole current source (A +) and a current drain (A -), the potential difference is

$$\varphi_2 - \varphi_1 = \frac{I\rho}{2\pi} ln\left(\frac{r_1}{r_2}\right) \tag{58}$$

In the case of a Four-Point Probe measurement, as shown in Fig. 4, the two external probes are used as a dipole current source and the remaining (internal) two, function as the voltage measurement probes. For an infinite sheet with equal spacing between all four probes we get a total potential difference of

$$\Delta\varphi = \frac{I\rho}{\pi} ln\, 2 \tag{59}$$
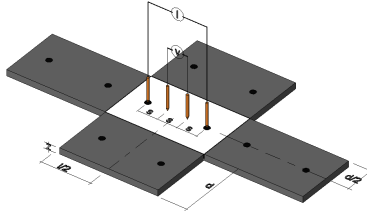
In this case the infinite sheet resistivity will be

Figure 4: *rectangular sample Four Point Probe setting*

$$\rho = \frac{V}{I}\frac{\pi}{ln\,2} \tag{60}$$

The problem of a finite sheet was treated by F.Ollendorff and Smits *[22]*. Employing similar techniques, we were able to compute an exact term of the electric potential for the suggested geometry and therefore compute the exact correction factor as displayed in Eq. 63. Our exact calculation was then compared to the one offered in the Smits calculation numerically. We introduce an infinite images to the original current source and drain, in such manner that the perpendicular component of the current at the boundary of all the images cancels completely due to the symmetry as shown in Fig. 5.
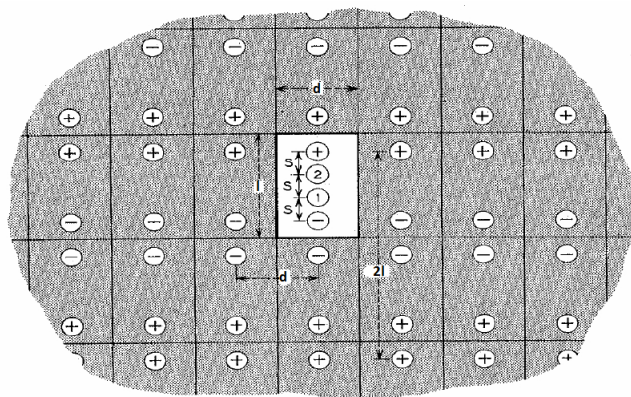

Figure 5: *A system of infinite images of the explored geometry*

We then sum the potential difference between the two inner probes due to the images. First step is finding a term for the spatial positions of voltage probes

$$\vec{r}_{nm}^{a} = (md, s + nl) \tag{61}$$

$$\vec{r}_{nm}^{b} = (md, nl - 2s) \tag{62}$$

Where the index (a, b) in the vector r (Eq. $61, 62$) stands for positive source location (a) and negative source location (b).

The potential difference between the two inner point is then achieved by a summation over all point sources

$$\Delta\varphi_{12} = 2 \times \frac{I\rho}{2\pi} \sum_{n,m} (-1)^n \left[ln\left(|r_{nm}^a|\right) - ln\left(|r_{nm}^b|\right) \right] \tag{63}$$

$$\Delta\varphi_{12} = \frac{I\rho}{2\pi} \sum_{n,m} (-1)^n ln \left(\frac{(md)^2 + (s + nl)^2}{(md)^2 + (nl - 2s)^2} \right) \tag{64}$$

The summation have shown very fast convergence as presented in Fig. 6, where different values of dimensions (l, d) have been chosen. Each line represents a different length, the horizontal axis represents different width and the distance between the contacts was chosen to be a constant of 2[mm].
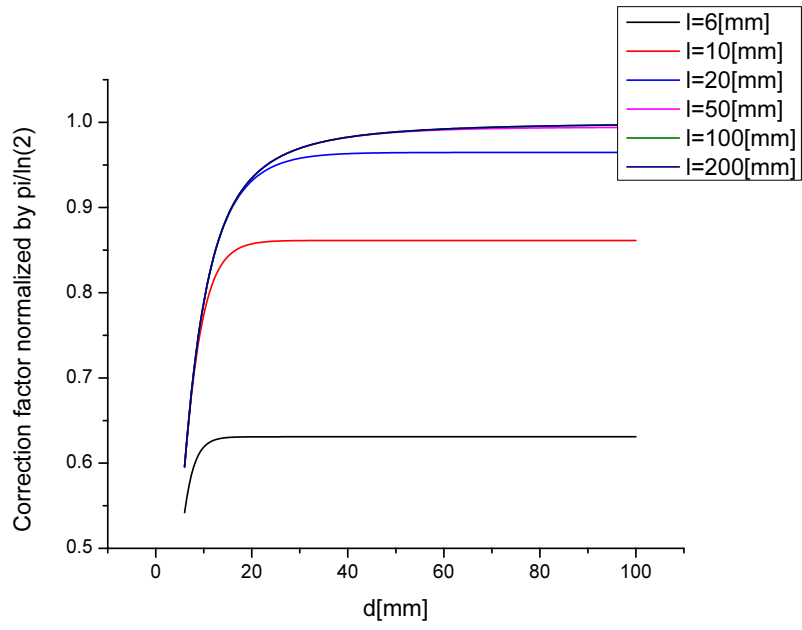
Figure 6: *The normalized correction factor of different dimensions.*

2 Experimental Method

2.1 Thin Film Deposition

In this work, thin superconducting films were deposited using Pulsed Laser Deposition (PLD). In the process, a high power pulsed Laser beam is focused onto a rotating target, inside a vacuum chamber as demonstrated in Fig. 7. We have used the third harmonic of Nd:YAG Laser with wavelength $\lambda \approx 355[nm]$,pulse duration of $10nsec$ with repetition rate of $10Hz$ which translates to $1[J/cm^2]$ average fluence on target. A rotating target absorbs the high energy Laser pulses in a very thin surface, and as a result the target material decomposes to a radiating (within the visible spectrum) jets of excited atoms and ions called plume. The rotation of the target prevents melting or overheating. This technique is usually done at ambient vacuum of $10^{-6}Torr$, for oxides growth, such as in this work. After a vacuum is achieved, a constant stream of oxygen is injected into the chamber while being pumped at the same time, maintaining constant $0.1Torr$ pressure . The plume is oriented towards the growth substrate which is preheated for $YBa_2Cu_3O_{7-\delta}$(YBCO) for example to 980^0C. The substrate is chosen to match to the lattice constant of the target material. We grow YBCO, $(Ca_xLa_{1-x})(Ba_{1.75-x}La_{0.25+x})Cu_3O_y$ (CLBLCO), $La_{2-x}Sr_xCuO_4$ (LSCO) and $Bi_2Sr_2Ca_{n-1}Cu_nO_{2n+4-x}$ (BSCCO) on $10 \times 10[mm^2]$ $SrTiO_3$(STO) with $c\,axis$ normal to the wafer.
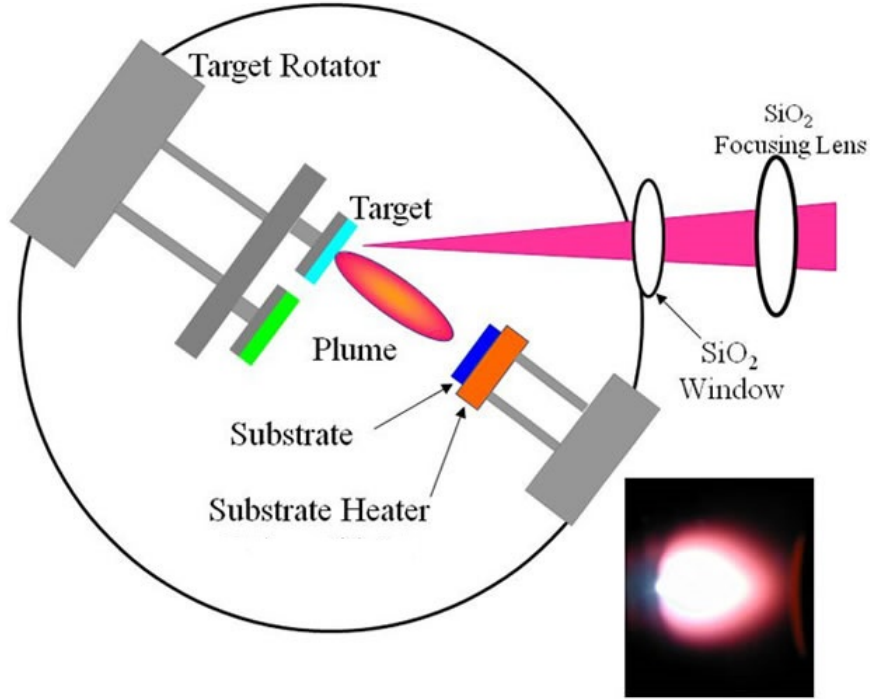
Figure 7: *PLD - Laser ablation system. In the right bottom corner a plume image presented.*

With these settings, the average growth rate can be estimated as $1.1\overset{o}{A}$ of single crystal layer per 10 Laser pulses. After the deposition the film is cooled down from 980^0C to 400^0C at rate of $1000\frac{Degrees}{Hour}$. When the film reaches 870^0C, the chamber is filled with Oxygen at $300[Torr]$ until a temperature of 400^0C is achieved. At this stage the doping is determined and the film is left for anneal at 400^0C, $300[Torr]$ for two hours, then the temperature drops at $600\frac{Degrees}{Hour}$ to room temperature.

2.2 Photo lithography - "Wet" & "Dry"

Every geometrical shape of deposited film in this work was made in a multistep process of photo lithography. After the target material is deposited on the STO wafer, we applied two layers of water-less positive photo-resist (PMMA) $0.5[\mu m]$ and $1.5[\mu m]$ thick coated with a spinner at 3000 and 5000 rpm respectively, then the PMMA is left for 20 minutes bake at 170^0C. Next, the sample is transferred into a deep UV mask aligner and exposed through the contact mask for 110 minutes. After the exposure, the photoresist is developed

in a MIBK solution then baked again for 20 minutes at 100^0C.

- **Wet etching -** Wet etching is obtained using acid reaction on the exposed areas (uncovered) that were previously patterned on the sample. Using HCl or HNO_3acid at concentration of 1% for 3 seconds followed by water wash to stop the reaction. The PMMA is then washed off with acetone, stream of nitrogen and finally isopropylene cleaning terminates the process.

- **Dry etching -** In this method we accelerate Ar Ions onto the sample that is glued with silver paste to a 45^0 tilted copper block holder. During the milling the sample is cooled to 190^0C using liquid nitrogen flow through the chamber to avoid over heating and rapid doping changes in the sample (oxygen loss). The argon ions are accelerated through $200[V]$ electric potential for a short "cleaning phase" and then under $500[V]$ throughout the process, in which the argon ions remove exposed film areas in a constant milling rate. Then a similar washing procedure is carried out. We present R Vs. T results obtained on bridges that were made in Gad Koren's laboratory in Fig. 10.

A common approach for absolute resistivity measurements includes bridge production, in order to eliminate the complex geometrical aspect of the relationship between resistivity and resistance. A bridge is a very narrow stripe of material connecting two infinite areas of material relatively to its width. In our first attempt to measure the absolute resistivity, we prepared several bridges like the one presented in Fig. 8 using wet etching. An AFM image of one bridge is shown in Fig. 9.
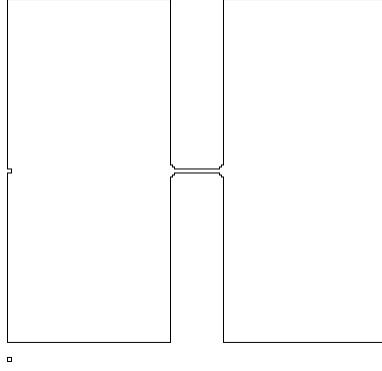
Figure 8: *A bridge contact mask design*
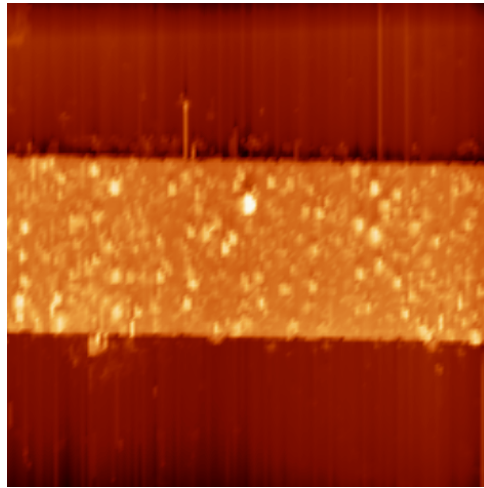
Figure 9: *A bridge AFM image top view*

A large deviation in the temperature dependent resistance measurement was found for these bridges as shown in Fig. 10. This result from spatial non uniformity in comparison to the bridge dimensions, and acid damages. We therefore abandoned the wet etching for thin films structures. We also found as discussed in details in sec.3.1, that dry etching has limitations. This lead us to use the *Four Point Probe Sheet Resistivity Measurement* discussed in the theoretical review.

Figure 10: *A Bridge resistance measurement - antinode direction wet etching production.*

2.3 Measurement System

The Resistivity Vs. Temperature measurement was made in the Four Point Probe technique, in this way contact resistance are eliminated and small resistive samples can be examined. Two outer probes flow constant curren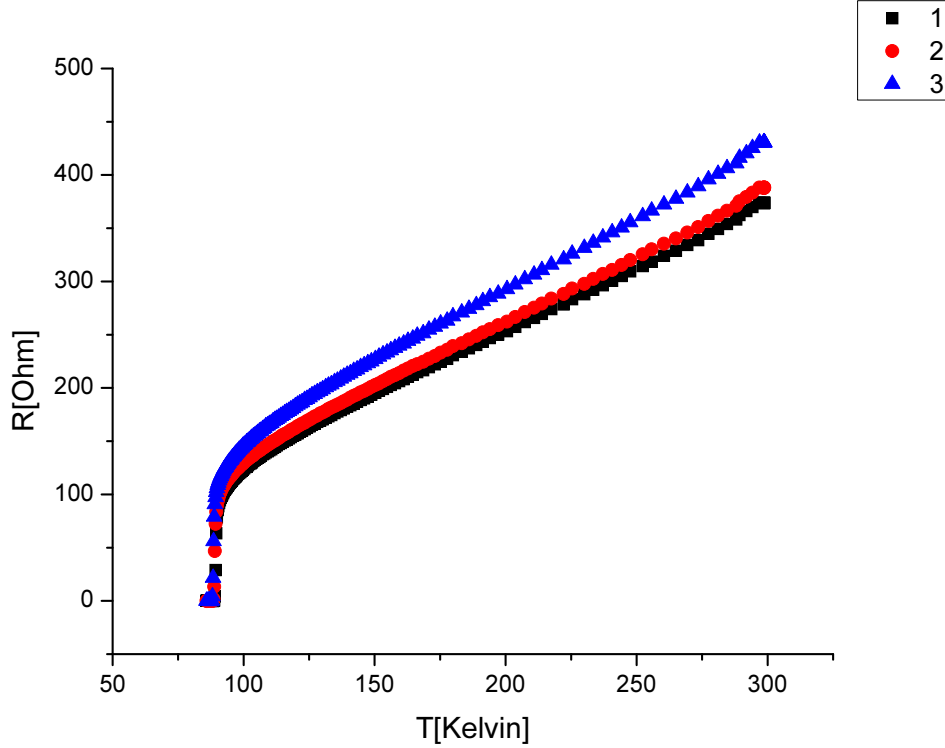t while the two inner probes measure the voltage as shown in the section 1.4, in this way, very little current passes through the voltage probe and the contact resistance which is varied in our contact structure as $50[\Omega]$ and is therefore negligible. The examined film was inserted into Oxford cryostat that is protected from the earth's magnetic field and other background fields using mu metal shield, the cryostat is then pumped to maintain low relative pressure and connected to a Helium Dewar in higher pressure relatively shown in the schematic diagram in Fig. 11, initiating Helium flow through a special layered tube into the cryostat. The temperature is probed and verified using two temperature detectors, one is a thermocouple based and

28

placed at the bottom of the cryostat and another one (diode) in proximity to the sample on the main sample probe.
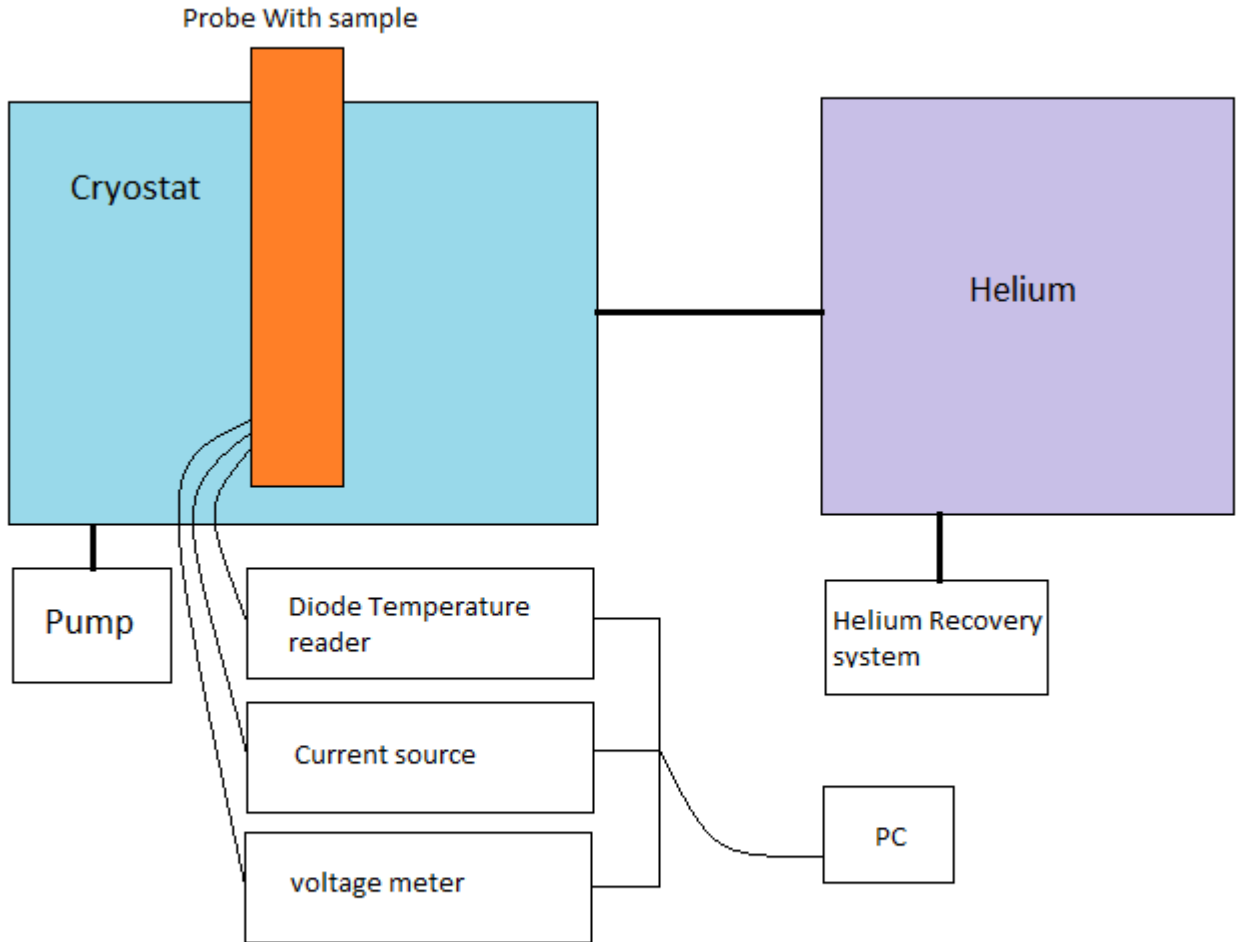
Figure 11: *A Schematic diagram of the R-T measurement system*

Our measurements are carried using constant current in toggle polarity mode, after verification of linear I-V plot in the current regime examined ($\sim 10 - 150 [\mu A]$). The Resistance was then calculated by $R = \frac{V}{I}$ numerically, for each temperature interval then averaged typically 10 times for each point in the Resistance Vs. Temperature (R-T)

curve. Finally, the resistivity was extracted by multiplying the resistance by the film height and geometric factor calculated for each film separately in the case of rectangular film measurement, or simply $\rho\left(T\right) = R\left(T\right)\frac{Height\times Width}{Length}$ in the case of a bridge. The film height and bridge width were measured using step measurement on the AFM as Shown in Fig. 12. Fig. 12 shows two different AFM step measurements done on the same sample taken from opposite sides revealing the same average height of 100 [nm].
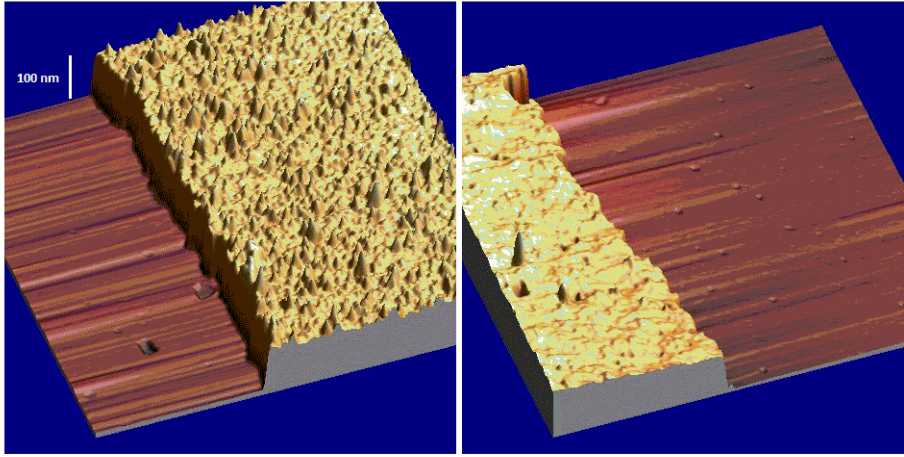
Figure 12: *A 3D AFM imaging of a step measurement*

3 Experimental Results

In this chapter we will present our main experimental results regarding absolute resistivity measurements on HTS's using thin films. The experimental data is composed of optimal doped YBCO, LSCO, BSCCO and CLBLCO, and divided into two main sections. The first section contains all YBCO measurements. We present results on different films with various heights, lengths, widths and distance between contacts. The raw data are factored with numerically calculated geometrical constant. and the validity of this procedure is checked. The second section contains LSCO, BSCCO and CLBLCO measurements.

3.1 Temperature Dependent Resistance-Resistivity Measurements on YBCO films

We present in Fig. 13 a simple I-V measurement of YBCO film of typical geometrical dimensions. The data is taken at several temperatures above T_c. A clear linear relation is demonstrated up to currents of 140 μA. All our subsequent measurements are done in a current of $100\mu A$, which is in the linear regime.
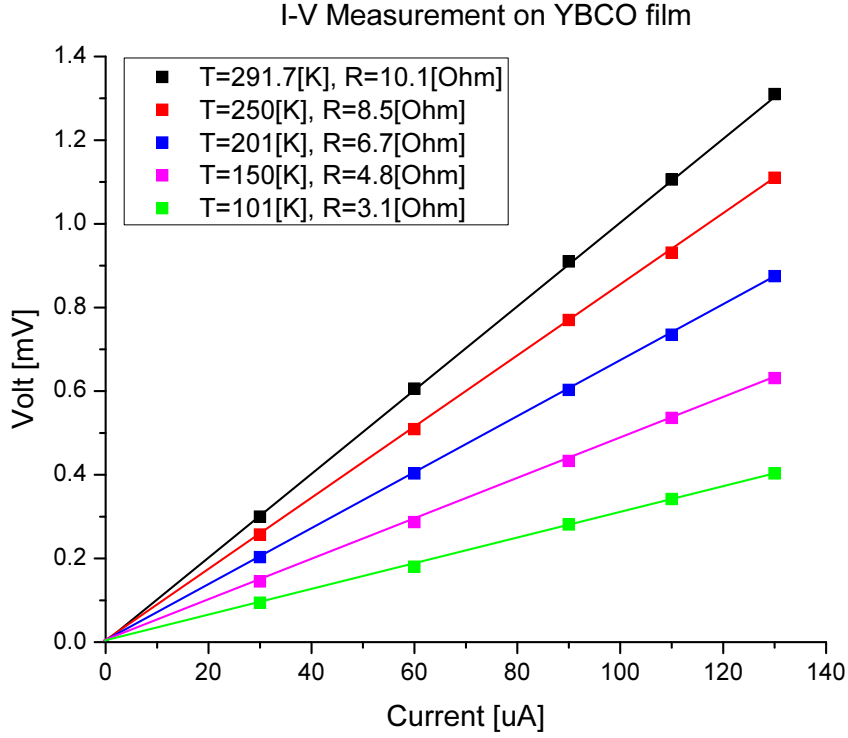
Figure 13: I-V Measurement at various temperatures on YBCO film

To check the validity of Eq. 63, we produced YBCO films of various geometries and measured their resistance as presented in Fig.14. Fig. 14 shows seven different films with height z, width d, length l and distance between contacts s, in units of millimeters. Layer (a) demonstrate the resistance before the geometrical scaling. Layer (b) is the resistivity extracted from the resistance employing the geometrical scaling. The linear, geometry independent, resistivity immediately above Tc is the most important part of our measurements.
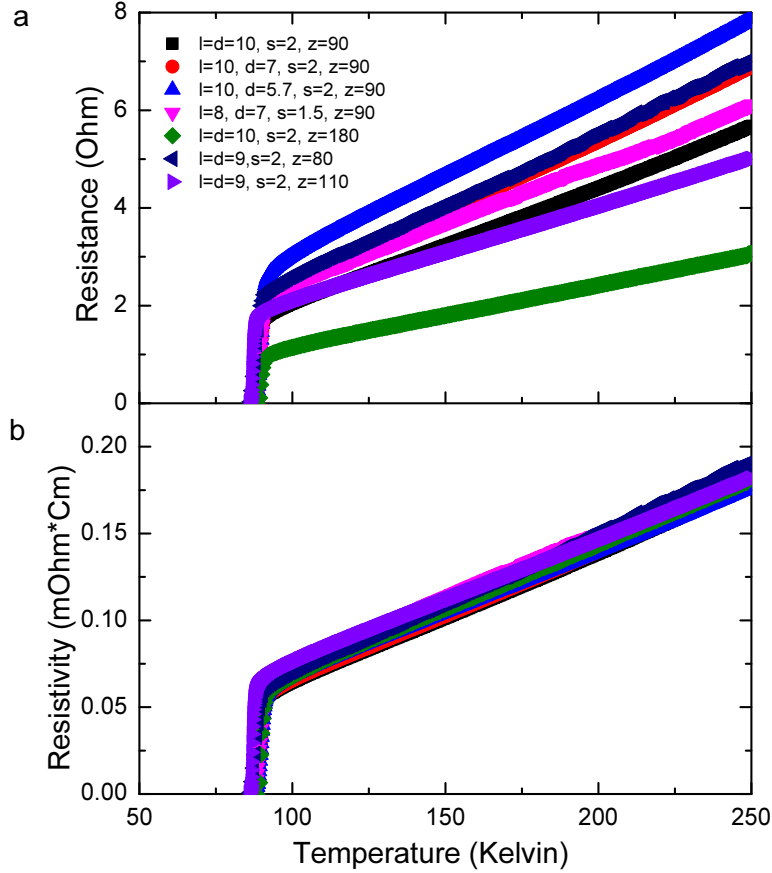
Figure 14: *YBCO thin films resistance measurements, raw data of the resistance (a) and resistivity after eliminating the geometrical dependency using the geometrical factor (b).*

Fig. 15 demonstrates the resistance for dry etched bridges. The resistance is measured on a series of bridges produced from the same wafer, and patterned in the same direction (anti-node/node). There is no justification of any correction factor in this case. Two elements are clear. For bridges, the transition is more rounded above T_c, and the scatter between one bridge to the next is not particularly good.

To quantify this aspect we took the derivative with respect to temperature for both films and bridges and generated a histogram. The normalized histogram is depicted in Fig. 16. A significant variance in the slope is shown for the bridges compared to films, which

demonstrates the ambiguity in defining the resistivity slope under T^*using bridges.
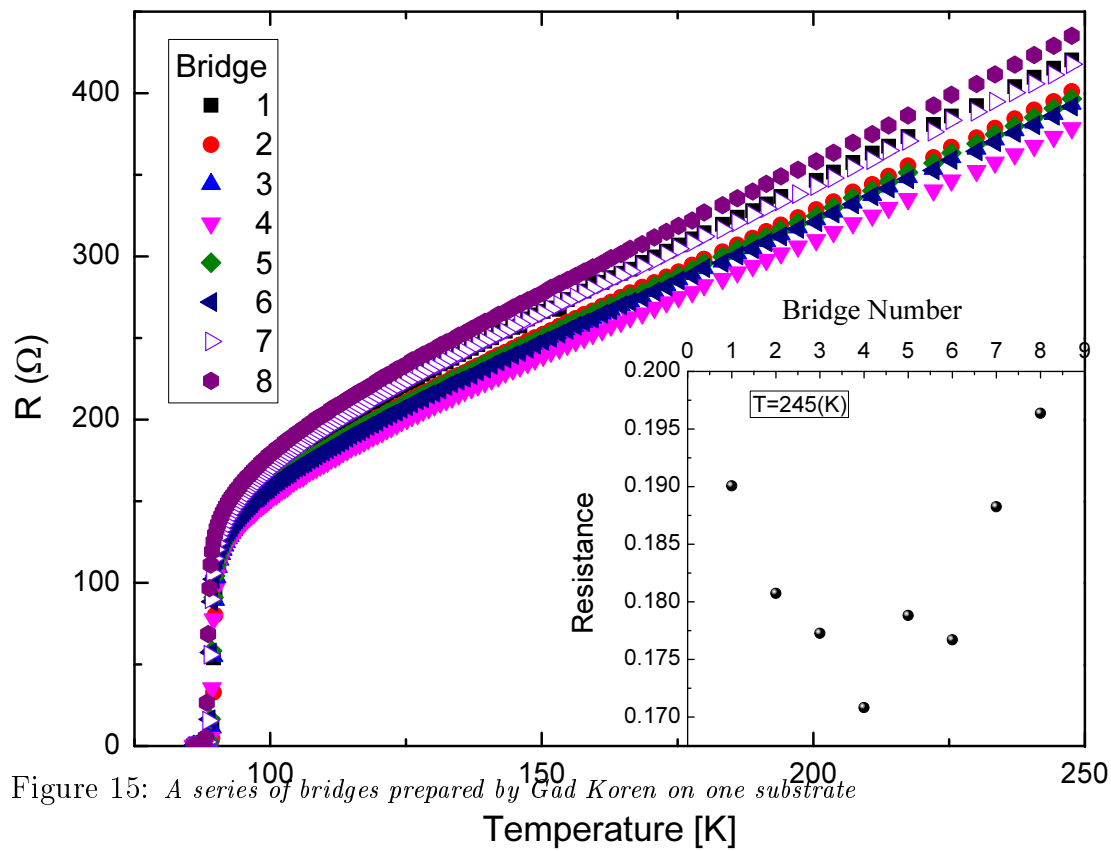
Figure 15: *A series of bridges prepared by Gad Koren on one substrate*
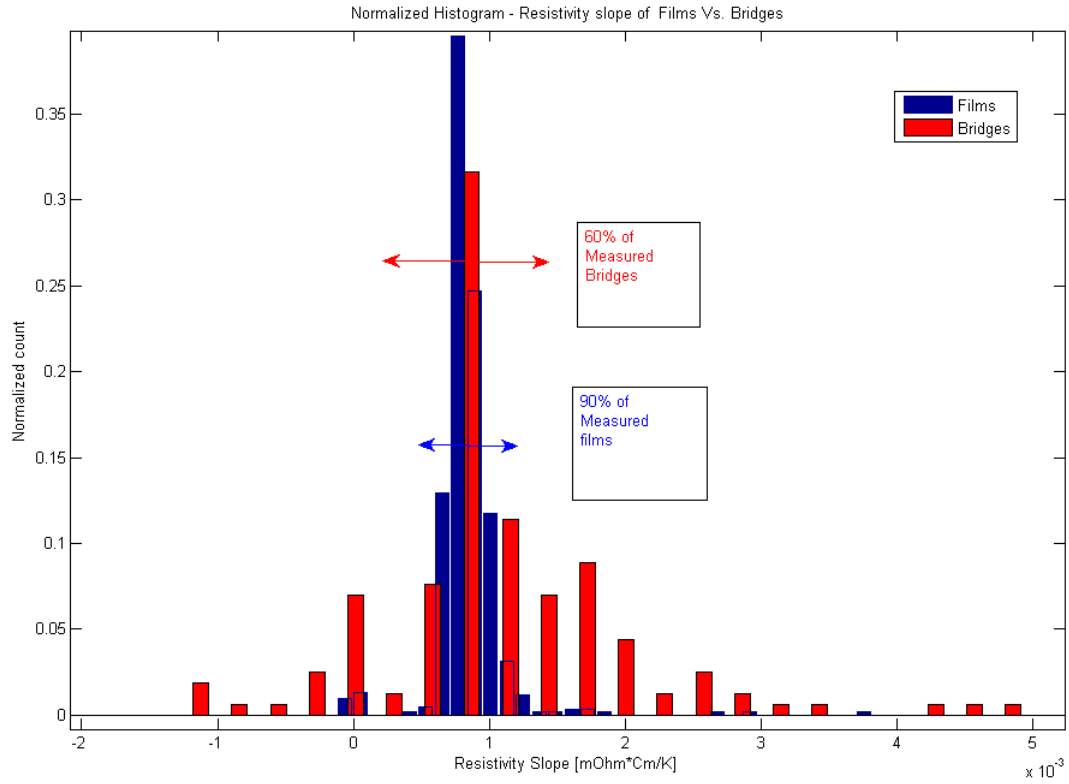
Figure 16: *A normalized histogram of the Temperature dependent resistivity slope , comparing between bridges and films.*

Since our main interest concerns the derivative of the resistivity with respect to temperature under T^* and above T_c in order to extract the HCB charge using the resistivity slope. Since films prove to give a more reliable result, all other measurements were made on thin films. These will be presented in the following section.
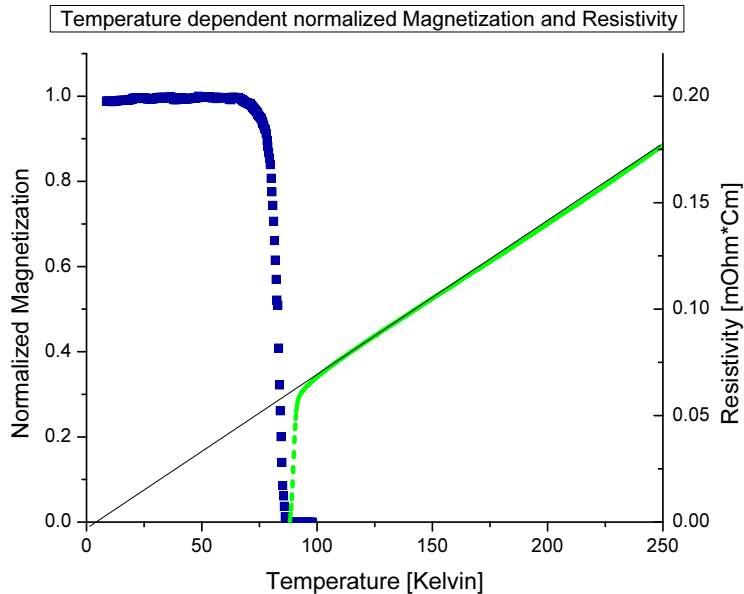
Figure 17: *Magnetization-Resistivity measurement of two different films, the magnetization is taken from a fraction of a film for homogeneity verification.*

In Fig. 17 we show temperature dependence of the resistance and magnetization of a typical YBCO film. $T_c = 88K$ defined by zero resistivity or zero magnetization agrees between the two methods and transition width of $4K$ is observed. Most important in this figure is the fact that the resistivity extrapolates to zero at zero temperature as expected in optimally doped YBCO. In addition, linear temperature dependence starts only ~10K above Tc. This is a unique property of YBCO films.

3.2   Absolute Resistivity Measurements on various HTSs

After achieving a measurement method for the absolute resistivity with lower variance of the slope with respect to the temperature, we have measured LSCO, BSCCO, and CLBLCO (x=0.1) as well, at optimal doping, as presented in Fig. 18. A pure linear behavior is observed only in YBCO. In LSCO the substrate reduces T_c from the bulk value considerably due to lattice parameters mismatch. To simplify our analysis we focus on the temperature range of 100 to 200 K which is higher than T_c, higher than the region

36
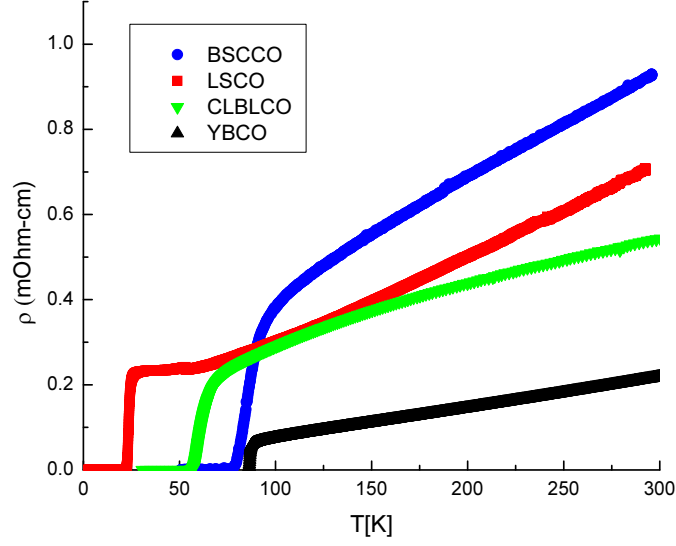
Figure 18: *LSCO,BSCCO,YBCO and CLBLCO absolute resistivity measurements*

of fluctuating superconductivity, and lower than T^* , for all materials.

Fig. 19 shows the first derivative of the resistivity as a function of temperature. As expected, the derivative is a constant only for YBCO. For other materials it varies with temperature but not by too much. We treat the derivative as a statistical variable and assign to each material an averaged resistivity slope and standard deviation.
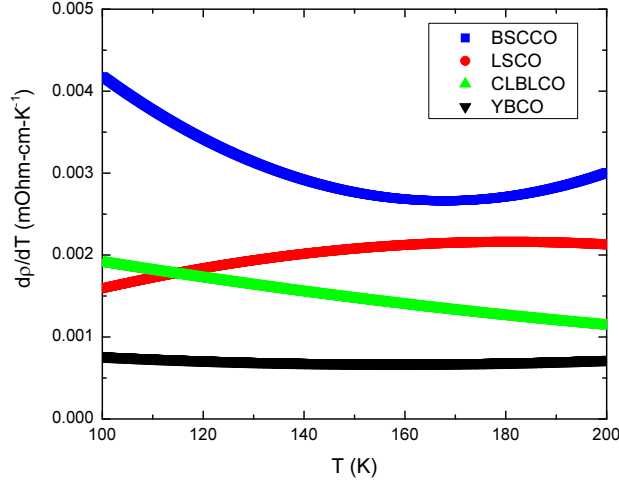
Figure 19: First derivative of to raw data.

Fig. 20 shows the average resistivity slope Vs. λ^2. The standard deviation is used to generate the error bars of $\frac{d\rho}{dT}$. The penetration depth is taken from previous μSR measurements. $Table\,1$ provides the λ values and the sources from which it was obtained. For YBCO λ was obtained in a theory free method using slow muons and the measurement error bar is known in this case. For the other materials the conversion from standard Muon spin relaxation to λ involves theoretical arguments and the error bar is not known.

Two straight lines are also give in Fig. 20. The LA line is based on Eq. 56 of section 1.3.6 with n_q=2. In the LA line there are no fit parameters. The "best-fit" line is the best linear fit to the data which passes through the origin. To convert the best fit to comprehensible unites we convert its slope to an effective boson charge n_q^{eff} ; $n_q^{eff} = 2 \cdot \sqrt{\frac{LA\ slope}{Fit\ slope}} = 1.72 \pm 0.15$. Notice that the best-fit line passes through the YBCO data point where the resistivity slope was independent of temperature.

	λ[nm]	Source
YBCO	146	[15, 17]
LSCO	210	[8][8]
BSCCO	270	[21]
CLBLCO	250	[16]

Table 1: *List of λ values Vs. sources in literature*
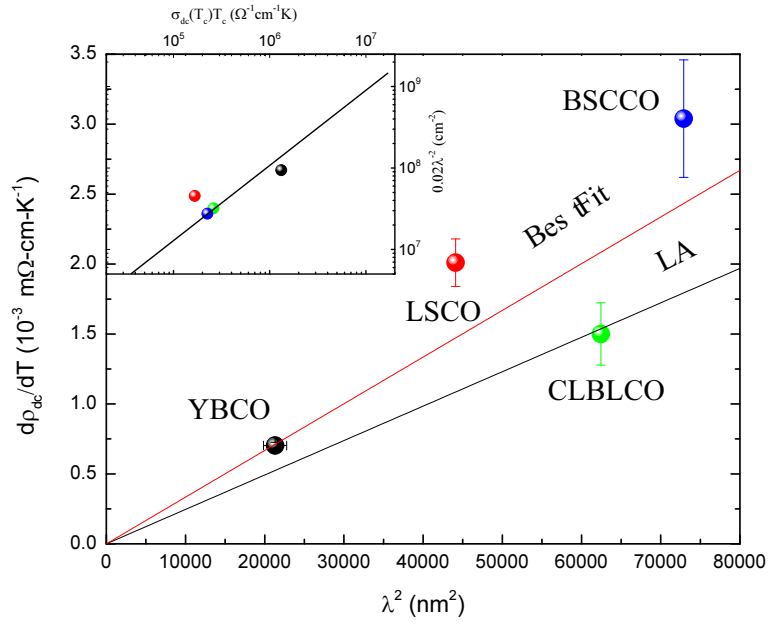
Figure 20: *The scatter of the resistivity slope Vs. λ^2, near T_c and far from it for various HTSs.*

4 Conclusions

The linear relations between the resistivity near the transition temperature, T_c, and under T^* for optimally doped YBCO; which is the cleanest cuprate was verified. The LA version of the Homes's law $\lambda^2(0) \propto \frac{d\rho_{dc}}{dT}(T_c)$ is also verified using different materials and on a linear scale. The acquired data was then analyzed and compared to the LA analysis of the HCB model (HCB) . The free parameter in this model is n_q, the mean effective charge of the hard core Bosons in the normal phase. If the model would have describe the materials perfectly, we should have found $n_q = 2$. We found $n_q = 1.72$. n_q is close to the model initial assumption of HCB with charge 2e. The model is therefore almost self consistent. This conclusion supports the growing belief and other experimental data in the existence of preformed pairs (cooper pairs) at temperatures above T_c [29, 24] .

However, the HCB model requires an additional theoretical work to describe better the cupratic HTS's dynamics. It is a disorder free model and does not take into account possible fermionic excitations above T_c and higher temperatures. It also overlooks anisotropy that is common among the examined cuprates [28, 27, 9, 2] and could possibly benefit by handling also doping variations.

5 Appendices

5.1 Appendix A - The definition of a fermionic state

Let us note the occupied state on the vacuum by $f_{i,\sigma_i}^\dagger |0\rangle = \phi_{i,\sigma_i}(r)$ when i, σ and r are lattice site numbering, spin polarization and position coordinate accordingly. Using these notations, an N fermion excited state is compactly written by Slater determinants

$$f_{N,\sigma_N}^\dagger ... f_{2,\sigma_2}^\dagger f_{1,\sigma_1}^\dagger |0\rangle = \begin{vmatrix} \phi_{1,\sigma_1}(r_1) & \cdots & \phi_{1,\sigma_1}(r_N) \\ \vdots & \ddots & \vdots \\ \phi_{N,\sigma_N}(r_1) & \cdots & \phi_{N,\sigma_N}(r_N) \end{vmatrix} |0\rangle \tag{65}$$

5.2   Appendix B - The Hubbard model and the strong interaction regime

5.2.1   The Hubbard Model

Maintaining the canonical fermion anti-commutation relations required $\left\{ f_{i,\sigma}, f_{j,\sigma'}^\dagger \right\} = 0$, and of course the annihilation operator on the vacuum ground state $f_{i,\sigma}|0\rangle = 0$ and defining the number operator, $n_i = f_{i,\sigma_i}^\dagger f_{i,\sigma_i}$ which counts the number of excitations per site. Now let us introduce our Hamiltonian, counting only states that account for particles exchange/hopping between nearest neighboring sites with no spin-spin interactions

$$\mathcal{H} = -\sum_{i,j} t_{ij} f_{i,\sigma}^\dagger f_{j,\sigma} \tag{66}$$

$$\mathcal{H} = \mathcal{H}_k + \mu \sum_i f_{i,\sigma}^\dagger f_{i,\sigma} = \sum_{i \neq j} t_{ij} f_{i,\sigma}^\dagger f_{j,\sigma} + \mu \sum_i f_{i,\sigma}^\dagger f_{i,\sigma} \tag{67}$$

Let t_{ij} be non zero for nearest neighbors only and add an attractive interaction between two charge carriers with opposite spin polarization in the z direction, as well as counting only for $i \neq j$ in the kinetic term while for $i = j$, the number, operator will be summing the occupation energy, hence, the chemical potential μ as written in (3).

Now let us take interest only on the kinetic term with the addition of an attractive interaction term between two electrons and equal hopping energy between nearest neighbors $t_{\langle i,j \rangle} = t$, o.w. zero

$$\mathcal{H} = -t \sum_{\langle i,j \rangle} \left(f_{i,\sigma}^\dagger f_{j,\sigma} + h.c. \right) - U \sum_i n_{i\uparrow} n_{i\downarrow} \tag{68}$$

The negative sign of the interaction constant U forces the formation of charge carrier pairs of opposite spin polarizations and the hermitian conjugate in the kinetic term represents the invariance of motion in all directions which is written due to the summation of

each interaction once in these notations in comparison to (2). This Hamiltonian is called "Negative U Hubbard Model". several polarization mechanisms have been proposed to explain this interaction amongst spin fluctuations (paramagnons) and lattice deformations (phonon) as mediators.

5.2.2 Strong Interaction Regime at Half Filling

We will consider the strong interaction regime, at low frequencies/temperatures, where the time scale for the polarization mechanism (the negative U interaction source) is considered to be immediate relatively to the hopping time. The negative U term favors local paring of spin up and down while the hoping term (t) competes with it and delocalizes electrons and as a result unbind pairs[3]. In this case we will consider the kinetic term as small perturbation to the pairing term up to second order $(U \gg t)$ and apply the Bouillon-Wigner perturbation theory[7]. For simplicity, we will deduce the bounded electrons coupling term considering two neighboring potential wells a,b. The Hilbert space is spanned by 6 possible configurations with the eigen states

$$|l\rangle = f_{a\downarrow}^{\dagger} f_{a\uparrow}^{\dagger} |0\rangle$$

$$|r\rangle = f_{b\downarrow}^{\dagger} f_{b\uparrow}^{\dagger} |0\rangle$$

$$|c\rangle = f_{a\uparrow}^{\dagger} f_{b\uparrow}^{\dagger} |0\rangle$$

$$|d\rangle = f_{a\downarrow}^{\dagger} f_{b\downarrow}^{\dagger} |0\rangle$$

$$|e\rangle = f_{a\downarrow}^{\dagger} f_{b\uparrow}^{\dagger} |0\rangle$$

$$|f\rangle = f_{a\uparrow}^{\dagger}f_{b\downarrow}^{\dagger}|0\rangle$$

The unperturbed Hamiltonian $\mathcal{H}_0 = -U\sum_i n_{i\uparrow}n_{i\downarrow} = -Un_{a\uparrow}n_{a\downarrow} - Un_{n\uparrow}n_{b\downarrow}$, with the eigenvalue $-U$ for states $|l\rangle, |r\rangle$ and zero energy for the states $|c\rangle, |d\rangle, |e\rangle\ and\ |f\rangle$. Assume $\mathcal{H} = \mathcal{H}_0 + V$, then $(\mathcal{H}_0 + V)|\psi\rangle = E|\psi\rangle$, and $|\psi\rangle = \sum_i c_i|i^0\rangle$ when $|i^0\rangle = |l\rangle, |r\rangle, |c\rangle, |d\rangle, |e\rangle, |f\rangle$, $c_i = \sum_j c_i^{(j)}$ and $E = \sum_j E^{(j)}$. Then

$$(\mathcal{H}_0 + V)|\psi\rangle = \sum_i c_i E_i|i^0\rangle + \sum_i c_i V|i^0\rangle = \sum_i c_i E|i^0\rangle \tag{69}$$

$$\sum_i c_i(E - E_i)|i^0\rangle = \sum_i c_i V|i^0\rangle \tag{70}$$

Multiply by $|\langle k^0|$ obtains

$$c_k(E - E_k) = \sum_i c_i \langle k^0|V|i^0\rangle \tag{71}$$

Define $V_{ki} = \langle k^0|V|i^0\rangle$ and rewrite the equation

$$c_k(E - E_k) = \sum_i c_i V_{ki} \tag{72}$$

For the ground states defined as $|g\rangle \to |l\rangle, |r\rangle$ we get at zero order the equations

$$c_l\left(E - E_l^{(0)}\right) = c_l V_{ll} + c_r V_{lr} + \sum_{m \neq g} c_m V_{lm} \tag{73}$$

$$c_r\left(E - E_r^{(0)}\right) = c_l V_{rl} + c_r V_{rr} + \sum_{m \neq g} c_m V_{rm} \tag{74}$$

The perturbation can relocate one fermion at a time, therefore

$$V_{im} = \langle i|f_{k,\sigma}^{\dagger}f_{j,\sigma}|m\rangle = 0\ \forall i, m \in l, r$$

44

All corrections in first order cancel this way.For $E = E_{r,l} + E^{(2)}$ in second order we get

$$E_r^{(2)} c_r^{(0)} = \sum_{m \notin g} V_{rm} c_m^{(1)} \qquad (75)$$

$$E_l^{(2)} c_l^{(0)} = \sum_{m \notin g} V_{lm} c_m^{(1)} \qquad (76)$$

Or counting on ground state with the index n

$$E_n^{(2)} c_n^{(0)} = \sum_{m \notin g} V_{nm} c_m^{(1)} \qquad (77)$$

To get $c_m^{(1)}$ we notice that for $m \notin g$ in first order we get the equation

$$\left(E_g - E_m^{(0)} \right) c_m^{(1)} = V_{ml} c_l^{(0)} + V_{mr} c_r^{(0)} \qquad (78)$$

And since $c_m^{(0)} = 0$ (no mixing between states at zero perturbation), we get

$$c_m^{(1)} = \sum_{n' \in g} \frac{V_{mn'} c_n^{(0)}}{E_g - E_m^{(0)}} \qquad (79)$$

$$E^{(2)} c_n^{(0)} = \sum_{m \notin g} \sum_{n' \in g} \frac{V_{nm} V_{mn'} c_{n'}^{(0)}}{E_g - E_m^{(0)}} \qquad (80)$$

Therefore the effective potential is

$$V_{nn'}^{eff} = \sum_{m \notin g} \frac{V_{nm} V_{mn'}}{E_g - E_m^{(0)}} \qquad (81)$$

This potential depends on the excited states yet works only on the ground states subspace. Defining projectors

$$P = \sum_{n \in g} |n\rangle\langle n| \quad 1 - P = \sum_{m \notin g} |m\rangle\langle m| \qquad (82)$$

45

And the effective potential

$$V_{eff} = \frac{V(1-P)V}{E_g - \mathcal{H}_0} \tag{83}$$

In the second order, the perturbation can switch between ground states, as calculated

$$V_{lr}^{eff} = V_{rl}^{eff} = -\frac{4t^2}{U} \tag{84}$$

thus we get the effective Hamiltonian

$$\mathcal{H}_{eff} = -\frac{4t^2}{U}\left(b_l^\dagger b_r + h.c.\right) - U\left(b_r^\dagger b_r + b_l^\dagger b_l\right) \tag{85}$$

When

$$b_r^\dagger|0\rangle = f_{a\uparrow}^\dagger f_{a\downarrow}^\dagger|0\rangle$$

$$b_l^\dagger|0\rangle = f_{b\uparrow}^\dagger f_{b\downarrow}^\dagger|0\rangle$$

With this definition it is easy to see that the 2nd term is solely composed of the number operators, which corresponds to $\mathcal{H}_0$, and the 2nd term to the pertubative hopping term in the original Hamiltonian. It is also easy to see that the fermionic pair obeys the bosonic canonical commutation relations

$$b_r^\dagger b_l^\dagger|0\rangle = f_{a\uparrow}^\dagger f_{a\downarrow}^\dagger f_{b\uparrow}^\dagger f_{b\downarrow}^\dagger|0\rangle = -f_{b\uparrow}^\dagger f_{a\uparrow}^\dagger f_{a\downarrow}^\dagger f_{b\downarrow}^\dagger|0\rangle = f_{b\uparrow}^\dagger f_{b\downarrow}^\dagger f_{a\uparrow}^\dagger f_{a\downarrow}^\dagger|0\rangle = b_l^\dagger b_r^\dagger|0\rangle \tag{86}$$

$$\implies \quad \left[b_l^\dagger, b_r^\dagger\right] = 0$$

Now considering low temperatures/frequencies we employ the reverse HP transformation upon the hopping term and achieve

$$\mathcal{H}_{hopping} = -\frac{4t^2}{U}\left(S_l^+ S_r^- + h.c.\right) \tag{87}$$

$$= -2\tilde{t}\left(S_r^x S_l^x + S_r^y S_l^y\right) \tag{88}$$

When $\tilde{t} = \frac{4t^2}{U}$ and the reverse HP transformation is

$$S_i^+ = (2s)^{1/2} b_i^\dagger$$

$$S_i^- = (2s)^{1/2} b_i$$

$$S_z = \hat{n}_i - \frac{1}{2}$$

The XY model is obtained. Considering interaction limited to nearest neighbors, we may expend this model to N body model consisting the kinetic term of the quantum XY model

$$\mathcal{H}_{Kinetic} = -2J\sum_{\langle i,j \rangle} S_i^x S_j^x + S_i^y S_j^y = -2J\sum_{\langle i,j \rangle} S_i^\perp \cdot S_j^\perp \tag{89}$$

when $J = -\frac{4t^2}{2}$ and $S^\perp = (S^x, S^y)$ the two dimensional spin vector on the XY plane. We may add a chemical potential to corresponding to the occupation parameter n_i and perform the reverse HPT

$$\mathcal{H} = -2J\sum_{\langle i,j \rangle} S_i^\perp \cdot S_j^\perp - \mu\sum_i S_i^z - \frac{1}{2}\mu\mathcal{N} \tag{90}$$

moreover, to include interaction between neighbors (mostly repulsive), we may introduce the *Ising anisotropy* coupling term

$$\mathcal{H} = -2J \sum_{\langle i,j \rangle} S_i^{\perp} \cdot S_j^{\perp} - \mu \sum_i S_i^z - \frac{1}{2} \mu \mathcal{N} + \sum_{\langle i,j \rangle} J_{ij}^{int} S_i^z S_j^z \tag{91}$$

5.3 Appendix C - Fluctuation dissipation relations

Let us define the anti commutator

$$\{A, B\} = AB + BA \tag{92}$$

and the interaction picture operator $\mathcal{O}^I$, as the operator $\mathcal{O}$ propagating in time with the unperturbed Hamiltonian evolution operator $U(t) = e^{-\frac{i}{\hbar}\mathcal{H}_0 t}$. Now, we define

$$f(\mathbf{q}, \omega) = i \int_{\infty}^{\infty} \langle [A^I(t), B^I(0)] \rangle e^{i\omega t} dt \tag{93}$$

$$g(\mathbf{q}, \omega) = \int_{\infty}^{\infty} \langle \{A^I(t), B^I(0)\} \rangle e^{i\omega t} dt \tag{94}$$

examine the operator averaged multiplication we get

$$\mathcal{I} = \int_{\infty}^{\infty} \langle B(0) A^I(t) \rangle e^{i\omega t} dt \tag{95}$$

$$= \int_{-\infty}^{\infty} \frac{1}{\mathcal{Z}} Tr \left\{ e^{-\beta \mathcal{H}_0} B e^{i\mathcal{H}_0 t/\hbar} A e^{-i\mathcal{H}_0 t/\hbar} \right\} e^{i\omega t} dt \tag{96}$$

$$= \frac{1}{\mathcal{Z}} \sum_{n,m} \int_{-\infty}^{\infty} e^{-\beta E_n} B_{nm} e^{iE_m t/\hbar} A_{nm} e^{-iE_n t/\hbar} e^{i\omega t} dt \tag{97}$$

$$= \frac{1}{\mathcal{Z}} \sum_{n,m} \int_{-\infty}^{\infty} e^{-\beta(E_n - E_m) - \beta E_m} B_{nm} A_{nm} e^{i(\omega + (E_m - E_n)/\hbar)t} dt \tag{98}$$

using the δ distribution twice we obtain

$$\mathcal{I} = e^{-\beta\hbar\omega} \int_{\infty}^{\infty} \langle A^I(t) B(0) \rangle e^{i\omega t} dt \tag{99}$$

plugging the result back to the predefined functions we get the relations

$$g(\mathbf{q}, \omega) = \frac{1}{2i} coth\left(\frac{\beta\hbar\omega}{2}\right) f(\mathbf{q}, \omega) \tag{100}$$

5.4   Appendix D - The BKT Transition

The *Berezinskii-Kosterlitz-Thouless* transition describes a low temperature quasi-ordered phase in which the correlations decrease as a power law with temperature. The 2D XY model exhibits U(1) continuous symmetry, when broken, Goldstone modes associated with this continuous symmetry logarithmically diverge with the system size hence destroying the expected phase transition with transverse fluctuations, as predicted by the Mermin-Wagner theorem for 2nd order phase transition. However, there exist a transition from exponential spatial correlations at high temperature to a power law correlations below a typical temperature T_{BKT}. This transition to a quasi-ordered phase with no long range order is of infinite order.

The BKT transition was seen in superfluid Helium films[23], superconducting arrays[1, 4][1, 4], superconducting films[6, 12] and more.

To get a further intuition on this transition, let us estimate the free energy of one vortex[6] employing the XY model Hamiltonian for very slow changes of order parameter in adjacent cells, $\mathcal{H} = -J\sum\limits_{\langle i,j\rangle} cos\left(\theta_i - \theta_j\right) \rightarrow cos\left(\theta_i - \theta_j\right) \approx 1 - \frac{1}{2}\left(\theta_i - \theta_j\right)^2 \approx 1 - \frac{a}{2}\left|\nabla\theta\right|^2$ where a is the lattice constant. The energy can be estimated by

$$E \approx \frac{\tilde{J}}{2}\int d^2x\left|\nabla\theta\right|^2 \tag{101}$$

Now, the condition for the existence of a topological defect is that if we circle the vortex at any distance, we will get an integer count (k) of the times θ rotates around itself, therefore

$$2\pi k = \oint \nabla\theta \cdot dl = 2\pi r\left|\nabla\theta\right| \tag{102}$$

assuming constant change of θ as a function of r. Now we can estimate the energy by

$$E \approx \frac{\tilde{J}}{2}\int d^2x\left|\nabla\theta\right|^2 = \pi Jk^2 ln\left(\frac{L}{\xi_0}\right) \tag{103}$$

where L is the lattice size and ξ_0 is the radius of the vortex core. Estimating the entropy associated with one vortex is done by the logarithm of the number of positions available for one vortex location given by areas ratio $S = K_B ln\left(\frac{L^2}{\xi_0^2}\right)$, so the free energy for k=1 of one vortex is given by

$$F = E - TS = 2ln\left(\frac{L}{\xi_0}\right)\left[\pi\frac{J}{2} - K_B T\right] \tag{104}$$

here we can see that above a certain temperature the free energy favors the existence of vortices and below it no (stable) vortices are allowed to obtain minimal value of F.

6   Bibliography

References

[1] David W. Abraham, C. J. Lobb, M. Tinkham, and T. M. Klapwijk. Resistive transition in two-dimensional arrays of superconducting weak links. *Physical Review B*, 26(9):5268–5271, November 1982.

[2] Yoichi Ando, Kouji Segawa, Seiki Komiya, and A. N. Lavrov. Electrical resistivity anisotropy from self-organized one dimensionality in high-temperature superconductors. *Physical Review Letters*, 88(13):137005, March 2002.

[3] Assa Auerbach. *Interacting Electrons and Quantum Magnetism*. Springer, September 1994.

[4] D. J. Bishop and J. D. Reppy. Study of the superfluid transition in two-dimensional he4 films. *Physical Review Letters*, 40(26):1727–1730, June 1978.

[5] J. Chang, N. Doiron-Leyraud, O. Cyr-Choiniere, G. Grissonnanche, F. Laliberte, E. Hassinger, J.-Ph Reid, R. Daou, S. Pyon, T. Takayama, H. Takagi, and Louis Taillefer. Decrease of upper critical field with underdoping in cuprate superconductors. *Nature Physics*, 8(10):751–756, October 2012.

[6] K. Epstein, A. M. Goldman, and A. M. Kadin. Vortex-antivortex pair dissociation in two-dimensional superconductors. *Physical Review Letters*, 47(7):534–537, August 1981.

[7] Eduardo Fradkin. *Field Theories of Condensed Matter Physics*. Cambridge University Press, 2 edition, February 2013.

[8] F. Gao, D. B. Romero, D. B. Tanner, J. Talvacchio, and M. G. Forrester. Infrared properties of epitaxial LSCO thin films in the normal and superconducting states. *Physical Review B*, 47(2):1036–1052, January 1993.

[9] J. Halbritter. Extrinsic or intrinsic conduction in cuprates: Anisotropy, weak, and strong links. *Physical Review B*, 48(13):9735–9746, October 1993.

[10] D. R. Harshman, R. N. Kleiman, R. C. Haddon, S. V. Chichester-Hicks, M. L. Kaplan, L. W. Rupp, T. Pfiz, D. Ll. Williams, and D. B. Mitzi. Magnetic penetration depth in the organic superconductor Î°-BEDT-TTFCu[NCS]. *Physical Review Letters*, 64(11):1293–1296, March 1990.

[11] K. Hashimoto, T. Shibauchi, T. Kato, K. Ikada, R. Okazaki, H. Shishido, M. Ishikado, H. Kito, A. Iyo, H. Eisaki, S. Shamoto, and Y. Matsuda. Microwave penetration depth and quasiparticle conductivity of PrFeAsO single crystals: Evidence for a full-gap superconductor. *Physical Review Letters*, 102(1):017002, January 2009.

[12] A. F. Hebard and A. T. Fiory. Evidence for the kosterlitz-thouless transition in thin superconducting aluminum films. *Physical Review Letters*, 44(4):291–294, January 1980.

[13] C. C. Homes, S. V. Dordevic, M. Strongin, D. A. Bonn, Ruixing Liang, W. N. Hardy, Seiki Komiya, Yoichi Ando, G. Yu, N. Kaneko, X. Zhao, M. Greven, D. N. Basov, and T. Timusk. A universal scaling relation in high-temperature superconductors. *Nature*, 430(6999):539–541, July 2004.

[14] C. C. Homes, S. V. Dordevic, T. Valla, and M. Strongin. Scaling of the superfluid density in high-temperature superconductors. *Physical Review B*, 72(13):134517, October 2005.

[15] H. Jiang, T. Yuan, H. How, A. Widom, C. Vittoria, and A. Drehman. Measurements of anisotropic characteristic lengths in YBCO films at microwave frequencies. *Journal of Applied Physics*, 73(10):5865 –5867, May 1993.

[16] Amit Keren, Amit Kanigel, James S. Lord, and Alex Amato. Universal superconducting and magnetic properties of the CLBLCO system, a muSR investigation. *Solid State Communications*, 126(1-2):39–46, April 2003.

[17] R. F. Kiefl, M. D. Hossain, B. M. Wojek, S. R. Dunsiger, G. D. Morris, T. Prokscha, Z. Salman, J. Baglo, D. A. Bonn, R. Liang, W. N. Hardy, A. Suter, and E. Morenzoni. Direct measurement of the london penetration depth in YBCO using low-energy muSR. *Physical Review B*, 81(18):180502, May 2010.

[18] L. Krusin-Elbaum, R. L. Greene, F. Holtzberg, A. P. Malozemoff, and Y. Yeshurun. Direct measurement of the temperature-dependent magnetic penetration depth in y-ba-cu-o crystals. *Physical Review Letters*, 62(2):217–220, January 1989.

[19] Netanel H. Lindner and Assa Auerbach. Conductivity of hard core bosons: A paradigm of a bad metal. *Physical Review B*, 81(5):054512, February 2010.

[20] Joseph Orenstein, G. A. Thomas, A. J. Millis, S. L. Cooper, D. H. Rapkine, T. Timusk, L. F. Schneemeyer, and J. V. Waszczak. Frequency- and temperature-dependent conductivity in YBCO crystals. *Physical Review B*, 42(10):6342–6362, October 1990.

[21] R. Prozorov, R. W. Giannetta, A. Carrington, P. Fournier, R. L. Greene, P. Guptasarma, D. G. Hinks, and A. R. Banks. Measurements of the absolute value of the penetration depth in high-tc superconductors using a low-tc superconductive coating. *Applied Physics Letters*, 77(25):4202 –4204, December 2000.

[22] Smits. Measurement of sheet resistivities with the four-point probe. *Bell System Technical Journal*, 34:711–718, 1958.

[23] V. E. Syvokon and K. A. Nasedkin. Dynamic phase transitions in a two-dimensional electronic crystal and in a two-dimensional helium film. *Low Temperature Physics*, 38(1):6, 2012.

[24] Tom Timusk and Bryan Statt. The pseudogap in high-temperature superconductors: an experimental survey. *Reports on Progress in Physics*, 62(1):61–122, January 1999.

[25] Michael Tinkham and Physics. *Introduction to Superconductivity: Second Edition (Dover Books on Physics)*. Dover Publications, 2 edition, June 2004.

[26] Y. J. Uemura, G. M. Luke, B. J. Sternlieb, J. H. Brewer, J. F. Carolan, W. N. Hardy, R. Kadono, J. R. Kempton, R. F. Kiefl, S. R. Kreitzman, P. Mulhern, T. M. Riseman, D. Ll. Williams, B. X. Yang, S. Uchida, H. Takagi, J. Gopalakrishnan, A. W. Sleight, M. A. Subramanian, C. L. Chien, M. Z. Cieplak, Gang Xiao, V. Y. Lee, B. W. Statt, C. E. Stronach, W. J. Kossler, and X. H. Yu. Universal correlations between tc and ns/m* (carrier density over effective mass) in high-tc cuprate superconductors. *Physical Review Letters*, 62(19):2317–2320, May 1989.

[27] D. A. Wollman, D. J. Van Harlingen, W. C. Lee, D. M. Ginsberg, and A. J. Leggett. Experimental determination of the superconducting pairing state in YBCO from the phase coherence of YBCO-Pb dc SQUIDs. *Physical Review Letters*, 71(13):2134–2137, September 1993.

[28] T. Xiang and J. M. Wheatley. Superfluid anisotropy in YBCO: evidence for pair tunneling superconductivity. *Physical Review Letters*, 76(1):134–137, January 1996.

[29] H.-B. Yang, J. D. Rameau, P. D. Johnson, T. Valla, A. Tsvelik, and G. D. Gu. Emergence of preformed cooper pairs from the doped mott insulating state in BSCCO. *Nature*, 456(7218):77–80, November 2008.

[30] H. C. Yang, L. M. Wang, and H. E. Horng. Characteristics of flux pinning in YBCO superlattices. *Physical Review B*, 59(13):8956–8961, April 1999.

תצפיות מודל בוזונים מקושחי הליבה
בעל מוליכות של הקופרטים

חיבור על מחקר

לשם מילוי חלקי של הדרישות לקבלת התואר
מגיסטר למדעים בפיסיקה

שחף ש. אסבן

1

תקציר

במחקר זה נדווח על מדידות התנגדות סגולית אבסולוטית תלויות טמפרטורה עבור מוליכי על בטמפרטורת גבוהות ובסימום אופטימלי מהסוגים, $La_{2-x}Sr_xCuO_4$, $YBa_2Cu_3O_{7-\delta}$, הדגמים . $Bi_2Sr_2Ca_{n-1}Cu_nO_{2n+4-x}$, $(Ca_xLa_{1-x})(Ba_{1.75-x}La_{0.25+x})Cu_3O_y$ נעשו בשכבות דקות [nm]80-180 וייצרו בדפוזיציה של פולסי לייזר. תשומת לב מיוחדת ניתנה לשיפוע ההתנגדות הסגולית כפונקציה של הטמפרטורה בין הטמפרטורת האופייניות T_c ו - T^*. התוצאות הושוו עם התאוריה של נתנאל לינדנר ואסא אורבאך ולגירסא התאורטית שנוסחה בעבודתם לחוק הומס (Homes Law) - $n_q^2 = 77.378 \frac{K_B}{\hbar c^2}\lambda^2(0)/\frac{d\rho}{dT}$, כך ש - $\frac{d\rho}{dT}(T_c)$ הוא שיפוע ההתנגדות הסגולית לפי הטמפרטורה הנמדד בסביבת טמפרטורת המעבר בתחום "הנורמלי" (במצב שאינו מוליך על), $\lambda(0), T_c$ הינם מרחק החדירה של השדה המגנטי לתוך המוליך בטמפרטורה אפס וטמפרטורת מעבר הפאזה בין מוליך על ל"נורמלי" בהתאמה, n_q הינו מספר יחידות מטען (e) חסר יחידות הנמצא בהגדרת "יחידת התנגדות" ($\frac{h}{(n_q e)^2}$ - Quanta of Resistance).

שתי תגליות חשובות נעשו בשלב מוקדם מאוד במחקר של מוליכות קופרטים (על מוליכים בטמפרטורת גבוהות). אחת היא ביחס לדגימות עם סימום נמוך (Underdoped), ביחסים הנמצאו ע"י Uemora $T_c \propto \lambda^{-2}$, T_c היא טמפרטורת המעבר ו - λ הוא עומק החדירה המגנטית. יחס זה נגזר באמצעות סיבוב ספין המיואון ומדידת השדה המקומי בתוך מוליך העל בעומקים שונים בטכניקה הנקראת μSR. התגלית השנייה הייתה כי בסימום נמוך ואופטימלי, בטמפרטורות T הגבוהות מטמפרטורת המעבר ונמוכות מטמפרטורה המוגדרת T^*, ההתנגדות הסגולית בעלת קשר לינארי לטמפרטורה $\rho \propto T$. בשלב מאוחר יותר הומס (Homes) גילה אמפירית קשר אחר המנוסח $\rho_s(0) \propto \sigma(T_c)T_c$ עבור סימום נמוך, אופטימאלי ואף גבוה כך ש-$\rho_s(0)$ מוגדר כצפיפות העל נוזל בטמפרטורה אפס וכן המוליכות מקיימת $\sigma(T_c) = 1/\rho(T_c)$ הנמדדת בקרבה לטמפרטורת המעבר (מלמעלה). קשר זה נתקבל ממדידת "מוליכות אופטית", פונקצית התגובה הליניארית לשדה חשמלי התלויה בתדר השדה. על מנת שיחסי יומורה וחוק הומס יתקיימו במקביל, מן ההכרח שהמוליכות בקירבה לטמפרטורת המעבר מלמעלה אליו תהיה גודל אוניברסלי משותף לכל החומרים בסימום נמוך. מודל תאורטי מהשנים האחרונות הנכתב ע"י אסא אוירבאך ונתנאל לינדנר, המתאר את המוליכות בחומרים הללו תחת השם "בוזונים מקושחי ליבה" (Hard Core Bosons - HCB) המקבל את ההתנגדות/מוליכות סגולית במסגרת המודל עבור טמפרטורות מעל הטמפרטורה הקריטית, בפאזה "הנורמלית", $\rho(T) = 77.378 \left(\frac{\lambda(0)}{n_q}\right)^2 \frac{K_B T}{\hbar c^2}$. במסגרת המודל, ההולכה מתבצעת ע"י בוזון (זוג קופר) בעל מטען 2e, כלומר $n_q = 2$ עד ספרה רביעית משמעותית.

מודל HCB צפוי להיות תקף לטמפרטורה נמוכה מ- T^* בה האמונה הגורפת כיום מתחילים להיווצר זוגות קופר. בשל זיהומים, בניסוי מסוים, יכול להיות שנצפה כי $\rho(T = 0) \neq 0$ ולכן נוח יותר להגדיר את חוק הומס הנובע מהמודל ע"י הנגזרת של ההתנגדות הסגולית לפי הטמפרטורה. משם ניתן למצוא מתוך הגדרת קוונטת ההתנגדות את המספר חסר היחידות המייצג את יחידות המטען האלמנטרי האחראי להולכה הפאזה "הנורמלית ע"י $n_q^2 = 77.378 \frac{K_B}{\hbar c^2}\lambda^2(0)/\frac{d\rho}{dT}$. מציאת n_q קרוב בערכו ל-2 יראה על קונסיסטנטיות עצמית של המודל ויראה אם המודל אכן התחלה טובה להבנת העל מוליכות של הקופרטים. על מנת לוודא שמדידות ההתנגדות בוצעו בתחום הליניארי של החומרים הנמדדים מבחינת יחס הפוטנציאל החשמלי לזרם, מדידות מתח-זרם נעשו על הדגמים בטמפרטורות שונות בין 300 קלווין ל-100 קלווין ונמצא עבור כל טמפרטורה קו לינארי המחבר את ערכי הזרם מול ערכי הפוטנציאל ומעגן את ההנחה העוקבת כי המדידות בתחום ה"אוהמי" (קשר לינארי בין מתח וזרם) של המערכת. על מנת להוציא את ערך ההתנגדות הסגולית, בטאנו את היחס

בין הפוטנציאל החשמלי הנמדד בדגם לבין הזרם המוזרם אליו (ההתנגדות) על ידי מכפלה של שתי פונקציות, אחת תלויה רק בגיאומטריה של הדגם הנמדד והשניה תלויה בתכונות עצמוניות של הדגם (ההתנגדות הסגולית). התחלנו ממדידת "גשרים", גשר הינו מבנה גיאומטרי צר נמוך וארוך מאוד באופן יחסי לשטח החתך. גשר הינו כלי נוח למדידת התנגדות סגולית שכן הפונקציה תלוית התכונות הגיאומטריות מנוונת לידי יחס אורך הגשר לשטח הפנים וע"י חלוקה בפקטור הנ"ל ניתן לחלץ את ההתנגדות הסגולית בצורה טריוויאלית. לאחר כמות מסוימת של מדידות כאלו, מצאנו כי רוחב מעבר הפאזה הינו רחב יחסית ולכן קיימת אי וודאות לגבי היכן ההתנגדות הסגולית המדוברת בחוק הומס אמורה להיות מדודה, הרי יש לקחת את הערך הקרוב ביותר למעבר הפאזה מלמעלה - בתוך תחום ההולכה הנורמלית, כמו כן מצאנו שפיזור ההתנגדויות המדודות גדול יחסית, כ-10% ולכן השגיאה במדידה תקשה על ההבחנה בין $n_q = 2$ לבין $n_q = 1$. לכן, החלטנו לנסות לעבור למדידות של פילמים שם ידוע כי מעבר הפאזה יותר צר. לאחר חישוב של הפונקציה התלויה בגיאומטרית הדגם (צורה, רוחב, אורך ועובי), מדדנו דגמים בצורות שונות ומימדים שונים. עבור כל דגם חישבנו את ערך פונקצית "התיקון" הגיאומטרי וע"י חלוקה של כל מדידת התנגדות תלוית טמפרטורה בנפרד קיבלנו שכל הגרפים קרסו לגרף אחד. המשמעות היא שאכן ביטלנו את השפעת הגיאומטריה ומערך המדידה ממדידת ההתנגדות והמידע המצוי ברשותנו הינו תלוי אך ורק בתגובת החומר הלינארית לשדה חשמלי מופעל עליו הלוא היא המוליכות/ההתנגדות הסגולית.

בשלב הבא, הכנו דגמים שונים מחומרים שונים ומדדנו עבור כל אחד מהם את ההתנגדות הסגולית, משם חישבנו את הנגזרת הנומרית של ההתנגדות הסגולית לפי הטמפרטורה ומצאנו פיזור נמוך מאוד באופן יחסי לפיזור הגשרים של מדידות שקולות. הוצאנו מספרות עדכנית את ערך עומק החדירה של השדה המגנטי בטמפרטורה אפס. את שני הערכים הללו הצבנו במשוואה העיקרית המתוארת מעלה ממנה אפשר למצוא את n_q ומצאנו ערך מספרי עבורו $n_q = 1.72 \pm 0.15$.

היחסים הלינאריים בין ההתנגדות הסגולית ליד טמפרטורת המעבר, T_c, ומתחת T^* עבור מוליכי על מסוממים אופטימלית אומת עבור כל חומר בנפרד. כמו כן, גרסתם של נתנאל לינדנר ואסא אוירבאך עבור חוק הומס $\lambda^2(0) \propto \frac{d\rho_{dc}}{dT}(T_c)$ אומתה גם כן. יחסים אלה הוכיחו לחומרים שונים ע"י מדידת שיפוע ההתנגדות הסגולית בדיוק מירבי. הנתונים שנתקבלו הושוו לספרות בתחום וכן לגרסת חוק הומס שפותח ע"י נתנאל לינדנר ואסא אוירבאך במסגרת מודל ה - HCB ונמצא כי $n_q = 1.72 \pm 0.15$. גודל זה נקרא בלשוננו מטען אפקטיבי ממוצע של הבוזון במודל. אם מודל זה היה מתאר את על המוליכים ממשפחת הקופרטים בצורה מושלמת הרי שהיינו מוצאים כי $n_q = 2$, אמנם הקרבה המספרית לערך זה מראה על קונסיסטנטיות עמצית של המודל ולכן מראה כי המודל הינו נקודת התחלה טובה להבנה של על המוליכות למשפחת הקופרטית בטמפרטורות גבוהות. זה תומך באמונה ההולכת וגדלה כי כבר מעל טמפרטורת המעבר בשלב בו צפיפות המצבים ליד אנרגית פרמי יורדת עם הירידה בטמפרטורה נוצרים זוגות קופר האחראים לחלק עיקרי מההולכה. עם זאת, מודל ה - HCB דורש עוד עבודה תיאורתית נוספת על מנת לתאר את הדינמיקה בצורה טובה יותר. מודל זה איננו כולל אי סדר, כמו כן, המודל איננו לוקח בחשבון עירורים פרמיונים (אקסיטציות של שני הפרמיונים היוצרים את הבוזון המתואר). המודל יכול כמו כן להיות שמיש במערכות מעבר לסימום אופטימלי אם יכללו בתוכו וריאציות סימום